SN-251
CS-72-5-1

ANALYSIS OF A SOLID PROPELLANT GAS GENERATOR USING AN AMMONIUM PERCHLORATE-POLYBUTADIENE COMPOSITE PROPELLANT

TECHNICAL REPORT, AFRPL-TR-72-58
MAY 1972

Prepared by: Douglas E. Coats
Gary R. Nickerson

ULTRASYSTEMS, INC.
FORMERLY DYNAMIC SCIENCE
2400 Michelson Drive
Irvine, California 92664

"APPROVED FOR PUBLIC RELEASE;
DISTRIBUTION UNLIMITED."

AIR FORCE ROCKET PROPULSION LABORATORY
AIR FORCE SYSTEMS COMMAND
UNITED STATES AIR FORCE
EDWARDS, CALIFORNIA

NOTICES

When U. S. Government drawings, specifications, or other data are used for any purpose other than a definitely related Government procurement operation, the Government thereby incurs no responsibility nor any obligation whatsoever, and the fact that the Government may have formulated, furnished, or in any way supplied the said drawings, specifications, or other data, is not to be regarded by implication or otherwise, or in any manner licensing the holder or any other person or corporation, or conveying any rights or permission to manufacture, use, or sell any patented invention that may in any way be related thereto.

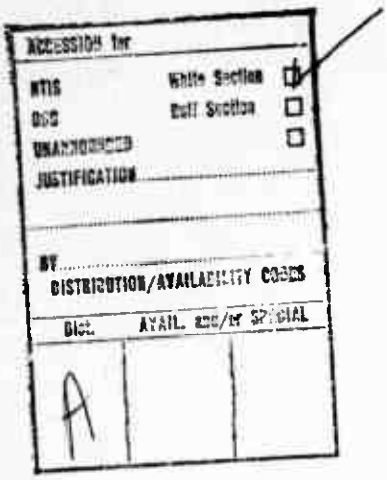

Unclassified

Security Classification

DOCUMENT CONTROL DATA - R & D

Security classification of title, body of abstract and indexing annotation must be entered when the overall report is classified)

1. ORIGINATING ACTIVITY (Corporate author) Ultrasystems, Inc. (formerly Dynamic Science) 2400 Michelson Drive Irvine, California 92664	2a. REPORT SECURITY CLASSIFICATION Unclassified 2b. GROUP

3. REPORT TITLE

ANALYSIS OF A SOLID PROPELLANT GAS GENERATOR USING AN AMMONIUM PERCHLORATE-POLYBUTADIENE COMPOSITE PROPELLANT

4. DESCRIPTIVE NOTES (Type of report and inclusive dates)

Final Report

5. AUTHOR(S) (First name, middle initial, last name)

Douglas E. Coats

Gary R. Nickerson

6. REPORT DATE	7a. TOTAL NO. OF PAGES	7b. NO. OF REFS
May 1972	71	26

8a. CONTRACT OR GRANT NO	9a. ORIGINATOR'S REPORT NUMBER(S)
F04611-71-C-0058 b. PROJECT NO 64100013148309	Technical Report AFRPL-TR-72-58
	9b. OTHER REPORT NO(S) (Any other numbers that may be assigned this report) SN-251/FR

10. DISTRIBUTION STATEMENT

This Document Approved for Public Release & Unlimited Distribution

11. SUPPLEMENTARY NOTES	12. SPONSORING MILITARY ACTIVITY
	Air Force Rocket Propulsion Laboratory Edwards, California 93523

An analytical program has been carried out for the purpose of studying the fluid dynamic and chemical processes occurring in a Solid Propellant Gas Generator (SPGG) device. The purpose of the SPGG device was to produce chemical exhaust species suitable for operation as a laser. The propellant used in the SPGG was Ammonium Perchlorate (AP) in a Polybutadiene (PBAN) fuel matrix. The combustion flame process was considered to occur in three successive steps: AP decomposition, PBAN pyrolysis, and combustion of the AP decomposition products with the PBAN pyrolysis products. For this combustion process a gas phase finite rate chemical reaction model was derived. Thirty chemical species were selected as a primary importance and a total of one hundred and fifteen reactions occurring between these species were considered. A survey of recent reaction rate data was conducted. Rates were selected from the results of the survey or were obtained from order of magnitude estimates. The combustion process occurring near the surface of the propellant was modeled in order to derive non-equilibrium. A small signal gain computation was incorporated into the computer model to allow computation of gain and broadening for specified transitions.

DD FORM 1473

Unclassified

Security Classification

14 KEY WORDS	LINK A		LINK B		LINK C	
	ROLE	WT	ROLE	WT	ROLE	WT
Laser						
Solid Propellant						
Rocket Exhaust						
AP Decomposition						
PBAN Pyrolysis						
Chemical Kinetics						

SN-251
CS-72-5-I

ANALYSIS OF A SOLID PROPELLANT GAS GENERATOR USING AN AMMONIUM PERCHLORATE-POLYBUTADIENE COMPOSITE PROPELLANT

TECHNICAL REPORT, AFRPL-TR-72-58
MAY 1972

Prepared by: Douglas E. Coats
Gary R. Nickerson

ULTRASYSTEMS, INC.
FORMERLY DYNAMIC SCIENCE
2400 Michelson Drive
Irvine, California 92664

AIR FORCE ROCKET PROPULSION LABORATORY
AIR FORCE SYSTEMS COMMAND
UNITED STATES AIR FORCE
EDWARDS, CALIFORNIA

FOREWORD

This is the final report furnished by Ultrasystems (formerly Dynamic Science) on the "Analysis of a Solid Propellant Gas Generator using an Ammonium Perchlorate - Polybutadiene Composite Propellant." The report was prepared for the Air Force Rocket Propulsion Laboratory, Edwards Air Force Base, California. It is submitted in accordance with the provisions of Air Force Contract F04611-71-C-0058 and has been assigned Dynamic Science Report Number CS-72-5-1.

Work presented in this report began in June 1971 and was concluded in Feb. 1972. The program was conducted within the Engineering and Computer Sciences Department of Dynamic Science at their Irvine facility. Mr. Douglas Coats was principal investigator on the program and was assisted by Messrs. G. R. Nickerson and H. M. Frey. The Air Force Program Monitor was Mr. J. Taska.

This technical report has been reviewed and is approved.

J. Taska
Project Engineer, AFRPL/LKCG

TABLE OF CONTENTS

1. INTRODUCTION

The purpose of this contract was to model the chemical combustion and mixing process in the Solid Propellant Gas Generator (SPGG) device and predict experimental conditions which were most favorable for laser action in the exhaust plume of the device.

The basic modeling tool to be used was Generalized Kinetic Analysis Program (GKAP), Reference 1, and the tasks involved were a) the establishment of a satisfactory kinetic combustion mechanism for the stream tube model, b) determination of an adequate model for the mixing process in the SPGG device, c) incorporation of the chosen models into the computer program, and d) comparison between analytical predictions and experimental observations

The propellant system in the SPGG is a composite made up of crystaline Ammonium Perchlorate (AP) in a Polybutadiene (PBAN) fuel matrix. Much of the effort under the contract was spent determining the initial composition of AP and PBAN in the gaseous state and determining a reaction set which would include most of the possible mechanisms for the combustion process. Section 2 of this report discusses the results of this effort. The mixing processes involved in propellants of this type were also extensively investigated and the model selected for the SPGG device is described in Section 3.

In order to compare with experimental measurements of electromagnetic gain, an option was incorporated into the GKAP computer code to calculate the small signal or zero power gain for the chemical system. The method of calculation is presented in Section 4.

Section 5 reports the results and conclusions arrived at from the total combustion model for the SPGG.

During the course of the contract, experimental data obtained by the Air Force determined that the SPGG device gave negative results in the measurement of gain. For this reason the emphasis on the work performed under this contract changed from a detailed analysis of the AP/PBAN propellant

system of the SPGG to adding a more complete laser modeling capability to the GKAP computer program.

Appendix A of this report describes two mixing models incorporated into the GKAP computer code during this contract and Appendix B shows the result of a H-F ignition study to verify the modeling capability of GKAP.

2. CHEMICAL MODEL FOR THE AP-PBAN SOLID PROPELLANT SYSTEM

The AP-PBAN solid propellant under consideration here consists of particles of crystalline ammonium perchlorate (AP) held in a matrix of polybutadiene (PBAN) binder. The weight ratio of AP to PBAN is approximately 70/30. Unlike rocket engine propellants, no aluminum metal is present. During the combustion process, the AP crystals are thought to act as a monopropellant producing a decomposition flame, which in turn pyrolizes the binder. The AP decomposition products and the products of the PBAN pyrolysis then react exothermically producing further combustion products. A flame model for this process is presented in Section 3.

In order to select a chemical model suitable for analyzing the AP/PBAN system, the combustion process has therefore been considered to occur in three successive steps. These steps are:

Step 1) AP decomposition

Step 2) PBAN pyrolysis

Step 3) combustion of AP decomposition products with the PBAN pyrolysis products

The purpose of this study is to attempt to predict by use of a kinetic model which gas phase species will result from the combustion process, and by what reaction mechanism will these species be produced. It is of particular interest to be able to identify reactions likely to take place which are highly exothermic and result in stable species. Species formed in this way will tend to populate excited states and therefore offer the possibility of either lasing directly or of transferring their energy to a species known to lase (such as CO_2). In order to establish a reaction mechanism for the AP/PBAN system it is necessary initially to consider the ground state chemistry. The results of the ground state analysis can then be used to indicate which excited state species are probable.

The chemical kinetics of combustion for a composite solid propellant are unknown at the present time. Solid phase reactions occurring at low temperature below the burning surface may be of importance in the initial stages of combustion. Reactions of this type are known to be complex since it is possible for many kinds of relatively stable molecules of increased molecular weight to be formed. What is of interest in this study, are the gas phase reactions which might lead to excited state species. Consequently a simple kinetic model has been adapted for the initial stages of combustion, which considers only gas phase reactions. The subsequent stages of combustion are assumed to occur at temperatures in the range known to exist in the AP/PBAN flame (the equilibrium flame temperature at 2.5 atm is 2219° K for the AP/PBAN used in this study).

The combustion chemistry of AP/PBAN composite propellant burning is only partly known at the present time. Accurate thermochemical data (e.g., JANNAF data) is available for most chemical species of interest, but the controlling chemical reactions are not known. It is possible, however, to postulate a system of chemical reactions sufficiently comprehensive to include many of the most important governing steps of the combustion process. The actual steps by which the postulated reactions proceed are open to question. In some instances excellent experimental reaction rate data is available, but for other reactions only theoretical estimates are available. Still other reactions have measured data available which is of unknown accuracy.

In attempting to compile a reaction mechanism for the combustion process, extensive use was made of the available literature. The literature on this subject, particularly concerning AP combustion, is massive. Nevertheless only part of the gas phase combustion chemistry for this system can be obtained from the literature. In order to fill in the missing parts of the reaction chemistry, reactions have been postulated which appear to be thermodynamically plausible. First the species to be considered were postulated. These are presented in Table 2-1. Certain reactions were then

TABLE 2-1

AP/PBAN SPECIES LIST WITH HEATS OF FORMATION, $\Delta H^{\circ}_{f_{298.15}}$

1	CH2	95.
2	CH2O	-27.7
3	CH3	31.9
4	CO	-26.4
5	CO2	-94.1
6	C2H	114.
7	C2H2	54.2
8	C2H4	12.5
9	CL	28.9
10	CLHO	-22.
11	CLO	24.2
12	CL2	0.
13	H	52.1
14	HCO	-9.
15	HCL	-22.1
16	HNO	23.8
17	HO2	5.
18	H2	0.
19	H2O	-57.8
20	N	113.
21	NH	79.2
22	NH2	40.3
23	NH3	-11.
24	NO	21.6
25	NO2	79.1
26	N2	0.
27	N2O	19.6
28	O	59.6
29	OH	9.9
30	O2	0.

eliminated due to steric and structural considerations, i.e., reactions involving the breaking and formation of several or bonds. Some reactions of this type (i.e., requiring much bond rearrangement) were retained because other investigators considered them important. Bond strengths were estimated using the JANNAF data. The bond dissociation energy, D, for molecule

BC

was taken as

$$D = (\Delta H_f^0 \text{ of B}) + (\Delta H_f^0 \text{ of C}) - (\Delta H_f^0 \text{ of BC})$$

where the heats of formation are at 298.15° K. These ΔH_f^0 are given in Table 2-1 for the species used in this study. The species are listed in alpha numeric order. A number of bond dissociation energies estimated in this way are presented in Table 2-2.

Particular attention was given so as to include reactions occurring between those species believed to be prevalent in the gas phase products. Reactions which occur by bond breakage through collision and involve minimal bond rearrangement were given high priority, regardless of whether the reaction was endothermic or exothermic. In other words emphasis was given to gas phase reactions at temperatures near the flame temperature.

Where it was necessary to estimate reaction rates, order of magnitude estimates were used. There are of course many methods by which reaction rates can be estimated. For example bond-energy-bond methods, collision theory methods, the Johnson and Parr method (Reference 2) and the Evans and Polanyi method (Reference 3) have all been used by various researchers.

The methods used in this study whenever reasonably reliable rate data was not available are presented below.

TABLE 2-2

BOND DISSOCIATION ENERGIES
ESTIMATES FROM JANNAF
(D kcal/mole)

D_{CH-O}	=	230.6	D_{H-H}	=	104.2
D_{CH_3-H}	=	101.9	D_{H-NO}	=	49.9
D_{Cl-Cl}	=	57.8	D_{H-O_2}	=	47.1
D_{Cl-O}	=	64.3	D_{N-H}	=	85.9
D_{ClO-O}	=	59	D_{NH-H}	=	91
D_{ClO_2-O}	=	48	D_{NH_2-H}	=	103.4
D_{ClO-H}	=	98.3	D_{N-N}	=	226.0
D_{Cl-OH}	=	55.9	D_{N-O}	=	151
D_{H-CO}	=	54.7	D_{NO-O}	=	2.1
D_{H-Cl}	=	103.1	D_{N-O_2}	=	33.9
D_{HC-CH}	=	229.8	D_{N_2-O}	=	40
$D_{H_2C-CH_2}$	=	177.5	D_{O-H}	=	102.3
D_{HCl-H}	=	111.9	D_{O-O}	=	119.2
D_{HCl-O}	=	112.9			

Order of Magnitude Arrhenius Equation Rate Estimates

When rate constants are represented by an Arrhenius equation, $k = AT^{-n} \exp(-E/RT)$, where T is the absolute temperature, R is the gas constant, A is the frequency factor, E is the activation energy, and n determines the pre-exponential temperature dependence, order of magnitude approximations have been made as follows:

Exothermic, trimolecular reactions

$$B+C+M \rightleftarrows BC+M \quad , \quad k = 3\times10^{16}\, T^{-0.5}$$

Exothermic, bimolecular reactions with triatomic transition states.

$$B+CD \rightleftarrows BC+D \quad , \quad k = 5\times10^{11}\, T^{0.5} \exp\left(-E/RT\right)$$

where E = 5.5% of the CD bond energy (Hirschfelder Rule, Reference 4)

Exothermic, bimolecular reactions with transition states of more than three atoms

$$BC+DE \rightleftarrows BCD+E \quad , \quad k = 1\times10^{11}\, T^{0.5} \exp\left(-E/RT\right)$$

where E = 5.5% of the DE bond energy

Exothermic bimolecular, binary exchange reactions

$$BC+DE \rightleftarrows BD+CE \quad , \quad k = 1\times10^{10}\, T^{0.5} \exp\left(-E/RT\right)$$

where E = 28% of the sum of the BC and DE bond energies

The reaction rates for the "spin forbidden" reactions can be similarly estimated if the rate constants are corrected by Boltzmann factors for the fact that these reactions do not occur in the ground state.

The above method of estimating exothermic reaction rates are similar to those used by Tunder, et al, Reference 5 .

AP Decomposition

The Decomposition and Combustion of Ammonium Perchlorate has been the subject of an enormous amount of research during the past 20 years. A systematic review of this subject through 1968 is given in Reference 6. The chemistry of this process must still be regarded as unknown to a large extent. Under conditions of interest in this study (steady state combustion at a pressure of several atmospheres) it has been determined, however, that an AP crystal initially undergoes dissociative sublimation consistent with the reaction:

$$NH_4^+ \quad ClO_4^- \quad (s) = NH_3\,(g) + HClO_4\,(g)$$

If the above reaction is assumed to occur near the AP crystal surface, the chemistry for the AP system reduces to an oxidation scheme for ammonia and for perchloric acid. Perchloric acid is known to be highly unstable and at the temperatures which exist near the surface of the propellant will rapidly decompose by the following steps:

$$HClO_4 \rightarrow ClO_3 + OH$$
$$ClO_3 \rightarrow ClO + O_2$$

Several chain reaction mechanisms initiated by the above steps have been given in the literature (for example References 6, 7, 8, and 9). For the purposes of this study it has been assumed simply that NH_4ClO_4 initially breaks down through the absorption of energy into equal moles of NH_3, OH, ClO, and O_2 according to the mechanism

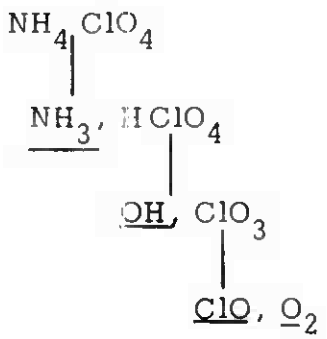

With these assumptions a kinetic model for the monopropellant combustion of AP consists of ammonia oxidation in the presence of ClO. The species which have been selected as being of possible importance are*

Cl
Cl HO
Cl O
Cl_2
H
H Cl
HO_2
H_2
H_2O
N
NH
NH_2
NH_3
NO
NO_2
N_2
N_2O
O
OH
O_2

*These species are those listed in Table 2-1 excluding species with carbon.

It is necessary to consider which chemical reactions between these species are likely to be the most important. For the ammonia species the the following reactions were selected as being of possible importance.*

$NH_3+Cl \rightleftarrows NH_2+H\,Cl$ (.335 kcal/mole)

$NH_3+ClO \rightleftarrows NH_2+Cl\,HO$ (5.150 kcal/mole)

$NH_3+H \rightleftarrows NH_2+H_2$ (- .762 kcal/mole)

$NH_3+O \rightleftarrows NH_2+OH$ (1.213 kcal/mole)

$NH_3+OH \rightleftarrows NH_2+H_2O$ (-15.890 kcal/mole)

$NH_3+O_2 \rightleftarrows NH_2+HO_2$ (56.340 kcal/mole)

The NH_3+OH reaction above is especially important because of the presence of large amounts of both species.

Many other reactions involving NH_3 are of course possible but have not been included for various reasons. For example the reaction

$NH_3+O_2 \rightleftarrows HNO+H_2O$ (- 23 kcal/mole)

has not been included because it is stearically complicated, involving breaking three bonds, and the activation energy is so high that it can not be an important step.

The reduction of NH_3 is followed by the reduction of NH_2 and of NH. Twenty three reactions have been included to account for this process and these are listed as reactions 74 through 96 in Table 2-4 at the end of this section. Table 2-4 contains the complete reaction table used in the

*The heat of reaction is taken as the sum of the $\Delta H^\circ_{f_{298}}$ of the products (RHS) minus the sum of $\Delta H^\circ_{f_{298}}$ of the reactants (LHS). Thus, if the sign is positive then the reaction is endothermic left to right, while if the sign is negative then the reaction is exothermic left to right.

study for the AP/PBAN system. The format and contents of Table 2-4 are discussed at the end of this section.

Other reactions occurring between the species selected for the AP system are listed as reactions 44 through 64, 67 through 73 and 101 through 119.

The above set of 74 reactions include all of the 21 reactions selected by McHale for AP combustion in Reference 10 with one exception. In the present study the reaction

$$CLO+CLO \rightleftarrows O_2+2Cl \qquad (+\ 9.5\ kcal/mole)$$

was used rather than

$$CLO+CLO \rightleftarrows O_2+CL_2 \qquad (-48.4\ kcal/mole)$$

since this reaction has been studied and found to proceed by the former path.

PBAN Pyrolysis

Fundamental studies on the pyrolysis of polybutadiene, such as presented in Reference 11, indicate that polybutadiene will pyrolyze into the same products as occur in chemical equilibrium. Results of equilibrium calculations at prescribed temperature and pressure are presented in Table 2-3. A total of 33 species were considered in these calculations. It can be seen that the major equilibrium products at the lower temperatures (600° K) are ethylene and acetylene. At higher temperatures (2000° K) ethylene tends to disappear but of course acetylene is very stable at high temperature. It has been estimated that the surface temperature for AP/PBAN composite propellants is approximately 600° C to 700° C regardless of pressure (Reference 12). At this temperature as can be seen from Table 2-3 the combined mole fraction of acetylene and ethylene represents 90% of the equilibrium product gases.

Experimental studies such as presented in Reference 11 show that the pyrolysis of PBAN results in formation in the following products:

vinylcyclohexane
butadiene
ethylene
acetylene

In other words the polybutadiene tends to pyrolyze into its dimer, monomer, and fragments of the monomer. It is easy to see how this might occur. The idealized chain structure for polybutadiene is

$$(\underset{1}{-}\ CH_2\ \underset{2}{-}\ CH = CH\ \underset{2}{-}\ CH_2\ \underset{1}{-})_n$$

TABLE 2-3

EQUILIBRIUM PRODUCTS FOR PBAN PYROLYSIS

ELEMENTAL COMPOSITION $C_{7.127}H_{10.94}O_{.111}N_{.151}$ PRESSURE = 2.5 ATM

Species	600°K	1000°K	1500°K	2000°K
	Mole Fractions			
CH_4	.000417	.086639	.110060	.005003
CO	.030559	.028724	.023087	.019766
C_2H	0	0	0	.001276
C_2H_2	.390947	.481691	.598472	.607228
C_2H_4	.556874	.377117	.066418	.003111
HCN	.000833	.011151	.019324	.020908
H_2	0	.000716	.176510	.338903
N_2	.003028	.013886	.006035	.002979

The weakest links in the chain are links 1 and 2.

link 1 = 41.9 kcal/mole
link 2 = 81.8 kcal/mole

Breakage at link 1 results in the monomer. Further breaks might then occur at link 2 such that

$$C_4H_6 \rightarrow C_2H_2 + 2\,CH_2 \rightarrow C_2H_2 + C_2H_4$$

The result is thus the formation of acetylene

$$HC \equiv CH$$

and ethylene

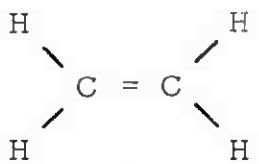

both of which are thermodynamically very stable.

Consequently, for the purposes of this study acetylene and ethylene were taken as the primary products of PBAN pyrolysis. The combustion chemistry is thus primarily the oxidation chemistry of these two species. In order to obtain kinetic mechanisms for the oxidation process, reference was made to the existing literature on the subject.

For acetylene the reaction mechanism and reaction rates given by Williams and Smith in Reference 13 were selected. This scheme is presented in Table 2-4 as reactions 2,23,24,30,31,32,33,34,35.

For ethylene the reaction mechanism and reaction rates given by Sorenson et. al. in Reference 14 were selected. This kinetic mechanism is a subset of their more comprehensive kinetic mechanism for ethane. This scheme is presented in Table 2-4 as reactions 7, 25,28,36, and 37.

Combustion of AP Decomposition Products with PBAN Pyrolysis Products

The complete AP/PBAN reaction set used in this study is presented in Table 2-4. In addition to the reactions discussed previously, this table contains reactions between AP and PBAN products. Also included are third body reactions between major species.

Reactions given in Table 2-4 include all of those reactions evaluated by the University of Leeds in References 15 (except for those reactions involving the H_2O_2 species). The species involved in these 12 reactions are: CO, CO_2, H, HO_2, H_2, H_2O, N, NO, NO_2, N_2, N_2O, O, OH, O_2.

Heats of reaction at 298.15°K for the reactions listed in Table 2-4 are presented in Table 2-5.

The format of Table 2-4 is as follows.

Each reaction is defined by one line of information. The information given on each line read left to right is:

Reaction; reactants = products

Rate (left to right); $k = A\ T^{-N}\ e^{-B/RT}$

with units of cc, mole, sec., °K, kcal

Reference

Reaction Number

The reactions have been divided into two types: those with an implied third body and those with no implied third body.

Implied Third Body Reactions

These reactions assume a third body to be involved in the collision process. For example reaction 1 is

$$CO + O + M = M + CO_2$$

where M represents any of the other species present in the system. In this study all third bodies were assumed to have the same efficiency. These reactions are listed in alphanumeric order by the species to be dissociated.

Reactions With No Implied Third Body

These reactions are listed in alphanumeric order by the principle species to be reduced.

TABLE 2-4. AP/PBAN REACTION SET

Implied Third Body Reactions

							SEQ
CO + O	=	CO2	A=5.05E15,	N=0.	B=2.5,	BAULCH (1968)L1	1
C_2H_2	=	C_2H + H	A=6.E14	N=0.	B=80.,	GARDINER (68)	2
CL + OH	=	CLHO	A=3.E16	N=.5	B=0.	ESTIMATE	3
CLO +H	=	CLHO	A=3.E16	N=.5	B=0.	ESTIMATE	4
HCL+ O	=	CLHO	A=3.E16	N=.5	B=0.	ESTIMATE	5
CL_2	=	CL + CL	A=2.E13,	N=0.	B=46.450,	SOLOMON(19_71)	6
HCO	=	H + CO	A=7.E13	N=0.	B=15.,	SORENSON(1971)	7
HCL	=	H + CL	A=6.86E21,	N=2.	B=102.17,	JACOBS (1966)	8
H + NO	=	HNO	A=4.E15	N=0.	B=.6,	BROKAW (19_70)	9
HO2	=	H + O2	A=2.40E15,	N=0.0	B=45.9	NO.36 BAULCH (1969)	10
H2	=	H + H	A=7.00E12,	N=-.50,	B=92.60,	NO.3 BROKAW (19_70)	11
H + OH	=	H2O	A=3.00E19,	N=1.00,	B= 0.00,	NO.5 PREHN (1967)	12
N + H	=	NH	A=3.00E16,	N=0.5	B= 0.0	NO.34 TUNOER (1967)	13
NH + H	=	NH2	A=1.80E16,	N=0.5,	B= 0.0	NO.33 TUNOER (1967)	14
NH3	=	NH2 + H	A=4.40E15,	N=0.0	B=79.5	NO.32 MICHEL (1965)	15
N + O	=	NO	A=1.00E20,	N=1.50,	B= 0.00,	NO.6 WRAY (1963)	16
N + O2	=	NO2	A=3.E16	N=.5	B=0.,	ESTIMATE	17
NO + O	=	NO2	A=2.00E15,	N=0.00,	B=-1.93,	NO.7 BROKAW (19_70)	18
N2	=	N + N	A=3.70E21,	N=1.60,	B=226.0,	NO.2 APPELTON (1968)	19
O + N2	=	N2O	A=1.00E18,	N=1.00,	B= 0.00,	NO.8 BORTNER (1967)	20
H + O	=	OH	A=2.E18	N=1.	B=0.,	CHERRY (1967)	21
O2	=	O + O	A=2.85E19,	N=1.00,	B=118.7,	NO.1 JOHNSTON (1968)	22

Reactions With No Implied Third Body

							SEQ
CH2 + O	=	HCO + H	A=3.E13	N=0.	B=0.,	BROWNE (1969)	23
CH2 + OH	=	HCO + H2	A=7.E13	N=0.	B=0.,	BROWNE (1969)	24
CH2O+ OH	=	H2O + HCO,	A=3.E14	N=0.	B=4.,	SORENSON(1971)	25
CH3 + O	=	CH2O+ H	A=1.9E13	N=0.	B=0.,	TUNOER (1967)	26
CH3 + O	=	HCO + H2	A=1.00E14,	N=0.00,	B= 0.00,	NO.15 BOWMAN (19_70)	27
CH3 + O2	=	CH2O+ OH	A=1.E11	N=0.	B=26.,	SORENSON(1967)	28
CH3 + O2	=	HCO + H2O	A=2.00E10,	N=0.00,	B= 0.00,	NO.13 BOWMAN (19_70)	29
C2H + O2	=	2*CO+ H	A=1.E13	N=0.	B=7.,	BROWNE (1969)	30
C2H2+ H	=	H2 +C2H	A=2.E14	N=0.	B=19.,	BROWNE (1969)	31
C2H2+ O	=	CO + CH2,	A=5.E12	N=0.	B=2.5,	BROWNE (1969)	32
C2H2+ O	=	OH +C2H	A=3.2E15	N=.6	B=17.,	BROWNE (1969)	33
C2H2+ OH	=	H2O +C2H	A=6.E12	N=0.	B=7.,	BROWNE (1969)	34

TABLE 2.4 AP/PBAN REACTION SET (continued)

C2H2+O2 = 2*CO+2*H	A=1.E14	N=0.	B=38.		GARDINER (68)	35
C2H4+ O = CH3 + HCO	A=2.5E12	N=0.	B=4.6		SORENSON(1971)	36
C2H4+ OH = CH2O+ CH3	A=5.E13	N=0.	B=6.		SORENSON(1971)	37
CO +CLO = CO2 + CL	A=1.E11	N=-.5	B=3.5		ESTIMATE	38
CO + O = CO2	A=1.78E10	N=0.	B=2.53		BAULCH (1968)L1	39
CO + OH = CO2 + H	A=5.6E11	N=0.	B=1.08		BAULCH (1968)L1	40
CO2 + H2 = CO +H2O	A=9.5E8	N=-.5	B=15.		TUNDER (1967)	41
CO2+ O = CO + O2	A=1.9E13	N=0.	B=54.15		BAULCH (1968)L1	42
CO2 + N = NO + CO	A=1.93E11	N=0.00	B= 3.40	NO.30	AVRAMENK(1965)	43
CL + HO2 = CLO + OH	A=5.E11	N=-.5	B=3.5		ESTIMATE	44
CL + HO2 = HCL + O2	A=5.E11	N=-.5	B=2.6		ESTIMATE	45
CL + H2 = HCL + H	A=1.2E13	N=0.	B=4.3		WESTONBERG (68	46
CL +NO2 = CLO + NO	A=5.E11	N=-.5	B=.1		ESTIMATE	47
CL + OH = HCL + O	A=2.0E11	N=-.67	B=.1		MAYER (1967)	48
CLHO+ CL = HCL +CLO	A=5.E11	N=-.5	B=5.1		ESTIMATE	49
CLHO+ H = H2O + CL	A=5.E11	N=-.5	B=3.1		ESTIMATE	50
CLHO+HCL = H2O +CL2	A=1.E10	N=-.5	B=43.5		ESTIMATE	51
CLHO+ N = HCL+ NO	A=5.E11	N=-.5	B=6.2		E TIMATE	52
CLHO+ O = CLO + OH	A=5.E11	N=-.5	B=3.1		ESTIMATE	53
CLHO+ O = HCL + O2	A=5.E11	N=-.5	B=6.2		ESTIMATE	54
CLHO+ OH = CLO + H2O	A=1.E11	N=-.5	B=5.4		ESTIMATE	55
CLO +CLO = O2 +2*CL	A=9.1E12	N=0.	B=0.		BAUER	56
CLO +CLO = CL2 + O2	A=1.E10	N=-.5	B=36.0		ESTIMATE	57
CLO+ H = HCL + O	A=5.E11	N=-.5	B=3.54		ESTIMATE	58
CLO+HO2 = CLHO+ O2	A=1.E11	N=-.5	B=2.7		ESTIMATE	59
CLO+ O = CL + O2	A=5.E11	N=-.5	B=3.54		ESTIMATE	60
CL2 + H = HCL + CL	A=3.0E14	N=0.	B=3.0		CHERRY (1967)	61
CL2 + H2 = 2*HCL	A=1.75E10	N=-.5	B=45.374		CHERRY (1967)	62
CL2 + OH = CLHO+ CL	A=1.E11	N=-.5	B=3.2		ESTIMATE	63
CL2 + O = CLO + CL	A=5.E11	N=-.5	B=3.2		ESTIMATE	64
HCO + CL = CO +HCL	A=9.E10	N=-.5	B=0.		TUNDER (1967)	65
HCO + OH = CO + H2O	A=1.00E14	N=0.00	B= 0.00	NO.17	ROWMAN (1970)	66
HCL + OH = H2O + CL	A=1.0E11	N=-.5	B=6.0		CHERRY (1967)	67
HNO+ CL = HCL+ NO	A=5.E11	N=-.5	B=2.75		ESTIMATE	68
HNO +HNO = N2O + H2O	A=1.E10	N=-.5	B=41.6		ESTIMATE *	69
HNO+ OH = H2O+ NO	A=1.E11	N=-.5	B=2.75		ESTIMATE	70
HO2 + N = NH + O2	A=1.E11	N=-.5	B=2.6		ESTIMATE	71
H2 + O = H + OH	A=2.96E13	N=0.00	B= 9.80	NO.19	BRABBS (1970)	72
H2 + OH = H + H2O	A=2.19E13	N=0.00	B= 5.15	NO.20	BAULCH (1968)	73
NH + CL = N + HCL	A=5.E11	N=-.5	B=4.7		ESTIMATE	74
NH +CLO = NO + HCL	A=1.E10	N=-.5	B=42.		ESTIMATE	75
NH + HNO = H2 + N2O	A=1.E10	N=-.5	B=38.0		ESTIMATE	76
NH + HNO = N2 + H2O	A=1.E10	N=-.5	B=51.7		ESTIMATE *	77

TABLE 2.4. AP/PBAN REACTION SET (continued)

NH + HO_2	= NH_2 + O2	A=1.E11	N=-.5	B=2.6	ESTIMATE		78
NH + NH	= N_2 + H2	A=3.60E_{11}	N=-.55	B= 1.9	NO.53 MAYER	(66)	79
NH + NO	= N_2 + OH	A=1.00E_{10}	N=0.5	B=66.2	ESTIMATE		80
NH + O	= NO + H	A=5.00E_{11}	N=-.5	B= 5.0	NO.35 TUNDER	(1967)	81
NH + O	= N + OH	A=8.40E_{12}	N=-.67	B= 0.1	NO.39 TUNDER	(67)	82
NH + OH	= H_2O + N	A=1.6E12	N=-.56	B=1.5	MAYER	(1967)	83
NH + OH	= NO + H2	A=1.E10	N=-.5	B=52.7	ESTIMATE		84
NH + O2	= H +NO2	A=1.E11	N=-.5	B=4.7	ESTIMATE		85
NH + O_2	= NO + OH	A=1.E_{10}	N=-.5	B=57.	ESTIMATE		86
NH2+ CL	= NH + HCL	A=1.E11	N=-.5	B=5.	ESTIMATE		87
NH2+CLHO	= NH3 +CLO	A=1.0E11	N=-.5	B=5.4	ESTIMATE		88
NH_2+CLO	= HNO + HCL	A=1.E_{10}	N=-.5	B=43.5	ESTIMATE		89
NH2+CLO	= NH +CLHO	A=1.E11	N=-.5	B=5.	ESTIMATE		90
NH2 + H	= NH + H2	A=1.70E11	N=-.56	B= 1.5	NO.40 MAYER	(66)	91
NH2 +HO2	= NH3 + O2	A=1.0E11	N=-.5	B=2.6	ESTIMATE		92
NH2 + NO	= N_2 + H_2O	A=.00E_{10}	N=0.5	B=75.0	ESTIMATE *		93
NH2 + OH	= NH + H_2O	A=3.00E_{10}	N=.70	B= 1.0	NO.42 TUNDER	(67)	94
NH2 + O	= NH + OH	A=9.00E11	N=.50	B=0.0	NO.41 TUNDER	(67)	95
NH2 +O2	= HNO + OH	A=1.0E10	N=-.5	B=59.	ESTIMATE		96
NH3 + CL	= NH2 + HCL	A=1.E11	N=-.5	B=5.7	ESTIMATE		97
NH3 + H	= NH2 + H2	A=2.00E11	N=.70	B=3.0	NO.44 TUNDER	(67)	98
NH3 + O	= NH2 + OH	A=1.50E12	N=0.0	B=6.0	NO.45 ALBERS	(68)	99
NH3 + OH	= NH2 + H2O	A=4.00E10	N=.70	B=1.0	NO.46 TUNDER	(67)	100
NO +HO2	= O2 +HNO	A=1.E11	N=-.5	B=2.6	ESTIMATE		101
NO + N	= N_2 + O	A=3.1E13	N=0.	B=.334	BAULCH (1969)	L4	102
NO + NO	= N_2 + O2	A=1.E13	N=0.	B=76.0	BAULCH (1969)	L4	103
NO2 + H	= NO + OH	A=7.20E14	N=0.00	B= 1.93	NO.28 SCHOFELD	(1967)	104
NO2+ HCL	= CLHO+ NO	A=1.E11	N=-.5	B=.1	ESTIMATE		105
NO2+ N	= NO + NO	A=1.E13	N=0.	B=0.	BAULCH (1969)	L4	106
NO2+ N	= N2O + O	A=1.E13	N=0.	B=0.	BAULCH (1969)	L4	107
NO2 + O	= NO + O2	A=1.E13	N=0.	B=.6	BAULCH ($19_7$0)	L5	108
NO2 + OH	= HNO + O2	A=1.E11	N=-.5	B=2.	ESTIMATE		109
NO2 + OH	= NO +HO2	A=1.E11	N=-.5	B=.1	ESTIMATE		110
N2O + H	= NH + NO	A=1.00E11	N=0.5	B=30.0	NO.49 TUNDER	(67)	111
N2O + H	= N2 + OH	A=3.00E13	N=0.00	B=10.80	NO.29 SCHOFELD	(1967)	112
N2O+ H2	= N2 +H2O	A=1.E11	N=-.5	B=2.2	ESTIMATE		113
N2O + O	= NO + NO	A=7.80E13	N=0.00	B=24.00	NO.24 SCHOFELD	(1967)	114
N2O + O	= N2 + O2	A=3.60E13	N=0.00	B=24.00	NO.26 SCHOFELD	(1967)	115
OH + OH	= O + H_2O	A=5.75E12	N=0.00	B= 0.78	NO.21 BAULCH	(1968)	116
OH + N	= H + NO	A=4.20E13	N=0.00	B= 0.00	NO.27 CAMPBELL	(1968)	117
O2 + H	= OH + O	A=1.44E14	N=0.00	B=16.60	NO.18 BELLES	(1970)	119
O2 + N	= O + NO	A=6.43E9	N=-1.0	B= 6.25	NO.23 BAULCH	(1969)	119

TABLE 2-5

HEATS OF REACTION AT 298.15°K, kcal/mole
(Listed by reaction number)

1	-127.193	2	-111.912	3	-60.354	4	-98.292	5	-59.496
6	-57.744	7	- 28.582	8	-103.087	9	-49.882	10	+47.102
11	-104.284	12	-119.332	13	- 95.982	14	- 91.002	15	+[illegible].442
16	-150.879	17	-105.09[illegible]	18	- 73.229	19	+226.000	20	- 39.949
21	-102.229	22	+119.118	23	-105.357	24	-107.332	25	- 42.430
26	-67.097	27	- 94.399	28	-50.208	29	-92.638	30	-114.738
31	+ 7.708	32	- 45.169	33	+ 9.683	34	- 7.420	35	- 2.626
36	- 43.015	37	- 17.688	38	-62.902	39	-127.193	40	- 24.964
41	+ 9.436	42	+ 5.075	43	- 23.786	44	- .300	45	- 55.985
46	+ 1.117	47	+ 8.938	48	- .850	49	- 4.795	50	- 58.978
51	-13.735	52	- 91.483	53	- 3.937	54	-59.622	55	- 21.040
56	+ 9.464	57	- 48.386	58	-38.796	59	- 51.190	60	- 54.827
61	- 45.243	62	- 44.126	63	- 2.513	64	- 6.447	65	- 74.505
66	- 90.750	67	- 16.245	68	-53.205	69	- 85.788	70	- 69.450
71	- 38.200	72	+ 1.975	73	- 15.128	74	-17.185	75	-103.873
76	- 83.390	77	-150.792	78	- 43.904	79	-158.400	80	- 91.348
81	- 65.077	82	- 16.327	83	- 33.43[illegible]	84	- 67.052	85	- 19.188
86	- 48.188	87	- 12.085	88	- 5.15[illegible]	89	- 62.753	90	- 7.290
91	- 13.202	92	- 56.340	93	-119.678	94	- 28.330	95	- 11.227
96	- 7.063	97	+ .355	98	- .762	99	+ 1.213	100	- 15.890
101	- 2.780	102	-75.021	103	- 43.160	104	-29.000	105	+ 13.733
106	- 77.750	107	- 41.741	108	- 45.889	109	+ 6.458	110	+ 9.238
111	+29.068	112	- 62.280	113	- 77.408	114	- 36.009	115	- 79.169
116	- 17.103	117	- 48.750	118	+ 16.889	119	- 31.861		

3.0 MIXING AND COMBUSTION MODEL FOR AN AMMONIUM PERCHLORATE AND POLYBUTADIENE COMPOSITE SOLID PROPELLANT

For most rocket motors, both solid and liquid propellants, it is assumed that the combustion products in the combustion chamber are in chemical equilibrium. Mixing is usually assumed to be complete or is handled by computing an O/F distribution across the chamber. The above assumptions are usually adequate for predicting rocket engine performance. However, the emphasis in the SPGG device is on the possibility of the development of substantial departures from chemical equilibirum in the combustion chamber which could also propagate to the exit plane of the nozzle. The two physical processes which determine the chemical composition in the chamber are the mixing rate between the fuel and oxidizer and the rate of chemical combustion (kinetics). Both of these processes are coupled together and depend on the physical characteristics of the device itself.

A schematic diagram of the SPGG device is shown in Figure 3-1. The device operates at a chamber pressure of 2.5 atmospheres with a contraction ratio of 53.3:1. The propellants are an ammonium perchlorate (AP) oxidizer (78% by weight) in a polybutadiene (PBAN) fuel matrix (22% by weight). The AP crystal size runs from 200 microns to 400 microns.

If the assumption of one-dimensional flow in chemical equilibrium is made, the velocity of the combustion product gases is 37.8 ft/sec at the propellant surface and the stay time in the nozzle is 3.2 milliseconds. From the velocity and equilibrium composition the Reynolds number in the chamber was estimated to be on the order of 5 to 10 based on AP particle sizes of 200 to 400 microns, respectively. Reynolds numbers in this range preclude turbulent mixing on the scale of the AP particle diameter due to viscous forces. Photographic data taken of the AP-PBAN propellant combustion process in the SPGG device also confirms the lack of turbulence on this scale. The motion picture show well established streamers many AP particle diameters above the propellant surface and are similar in nature to columnar diffusion flames. However, it is not possible to determine if the visible streamers are part of primary or secondary combustion zone without accurate temperature measurements. With the presence of apparent columnar diffusion

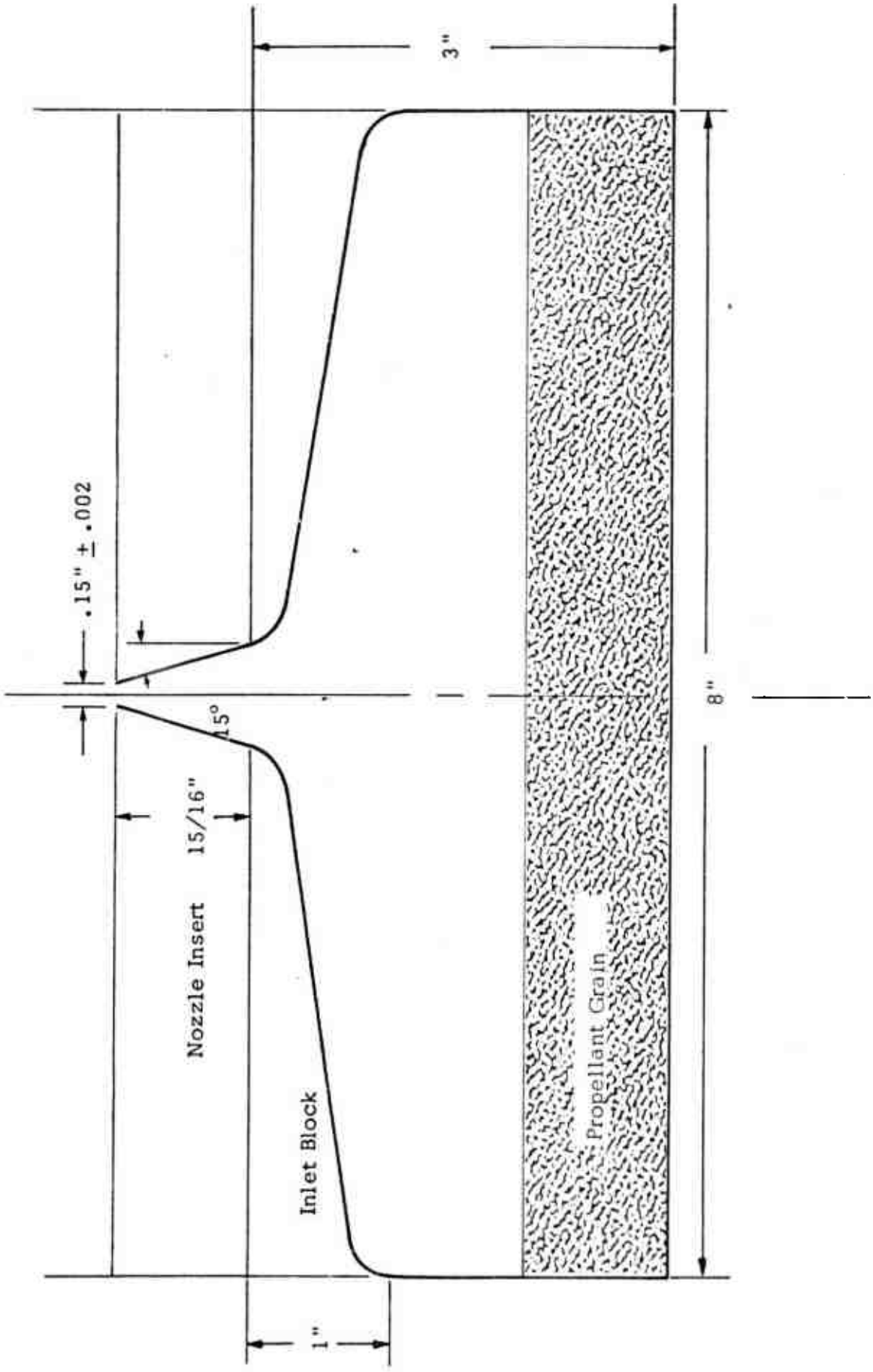

Figure 3-1. SPGG Device Schematic

flames, it is tempting to assume a laminar diffusion flame model to describe the mixing and kinetics. Unfortunately, however, there are two main drawbacks to this approach, the first is that the columnar diffusion flame theory predicts that the height of the flame zone, i.e., the height at which the temperature of the gas becomes approximately the equilibrium flame temperature, is independent of pressure, which is in contradiction with experimental data and conclusions of References 16, 17, 18, 19. The second drawback is that there is no a priori method of establishing the composition and energy content of the fuel and oxidizer streams. It becomes apparent then, that any rigorous treatment of the problem of composite propellant burning must consider the interaction between the combustion flames and the propellant surface.

This very problem, the steady state combustion of composite propellants, has been studied extensively for years. However, despite the large amounts of experimental and theoretical research done on this problem, no definitive model has been advanced which is capable of accurately predicting the combustion characteristics and flame structure of a composite solid propellant.

Most of the models proposed to date Ref. 16, 17, and 18 are multi-flame models and are for small oxidizer grains (3 to 20 microns), moderate to high pressures (100 psia and greater), and are intended to predict the linear burning rate of the composite propellant. However, in the SPGG device, we have noted that the oxidizer grain size is quite large (200 to 400 microns), and the pressure low (2.5 atm), so that the applicability of the models proposed becomes unclear. Another disadvantage of the models proposed in the literature is that they are essentially one-dimensional in nature and ignore or gloss over the details of the mixing process between the gaseous fuel and oxidizer. The mixing process, however, is precisely the point of interest for the SPGG device since we are looking for nonequilibrium effects which could be caused by mixing.

In addition to the mixing, the source of energy needed to perform the endothermic pyrolysis of the fuel binder must be known in order to establish the energy content of the fuel and oxidizer in the gaseous state. The possible sources of this energy by way of conductive heat transfer and combustion are shown in Figure 3-2 and are:

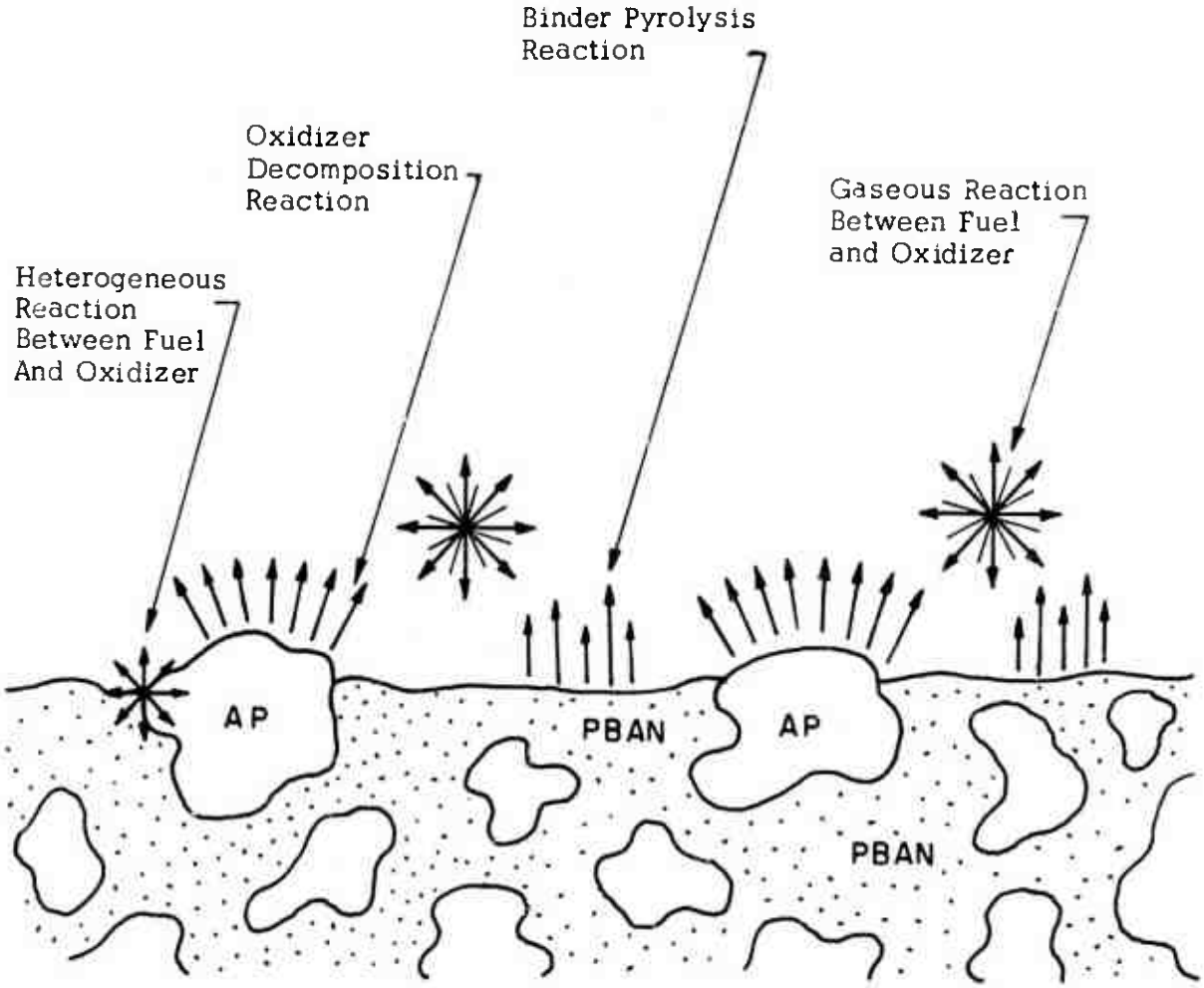

Figure 3-2. Illustrative Schematic of Combustion Processes In An AP/PBAN Composite Solid Propellant

1. Exothermic decomposition of the oxidizer crystal.
2. Exothermic gas phase reactions between the oxidizer decomposition products and the fuel pyrolysis products.
3. Exothermic heterogeneous reaction between the binder and the oxidizer interface.

The rate controlling step for the combustion process, while not known exactly, must consist of one or more of the following:

a. Chemical reaction kinetics occurring in the various reaction zones.
b. Mixing (diffusive and/or convective) between the oxidizer decomposition products and fuel pyrolysis products.
c. Conductive heat transfer from the flame into the propellant surface.

Unfortunately, there is a lack of agreement (e.g. Reference 19 and 20) in the results of experiments designed to determine the structure of the flame zone. It is particularly important to determine by measurement the temperature profile above and below the propellant surface. This knowledge is necessary in order to determine the importance of solid phase reactions in sustaining the combustion process and to answer questions regarding the transfer of energy from gas phase chemical reactions to the prepellant surface. Experimental results to date are not sufficiently accurate to provide this type of temperature profile data. These results do show, however, that temperatures near the equilibrium flame temperature for the mixture occur very close to the propellant surface.

Reference 17 has proposed a three flame model for composite propellant burning. The model consists of an AP deflagration flame extending from the surface, a primary flame between the AP decomposition products and the PBAN pyrolysis products, and a final or secondary diffusion flame between the basically oxidizer and fuel streams. This model would fit nicely with the observations of the combustion process in the SPGG device. While the model is essentially one-dimensional with the two-dimensional effects accounted for by varying the time constants for the various physical mechanisms involved, it has great appeal if a reasonable method could be established to determine the enthalpy and composition of the first two flames. To

determine if a reasonable method is obtainable, it is necessary to get an estimate on the amounts of energy transferred.

A simple equilibrium model was used to determine the amount of energy required to pyrolyze the fuel binder. In this model it was assumed that the gaseous fuel products were in equilibrium at the surface temperature (also pyrolysis temperature) of the fuel. The surface temperature of the fuel was taken as 600°C, Ref. 11 , and it was found that approximately 1250 cal/gm of heat addition was necessary to pyrolyze the fuel. This result compares favorably with estimates made from the activation energy of PBAN. The same type of calculation was performed for AP and it was found that the AP equilibrium products at the surface temperature of propellant had an enthalpy of 173 cal/gm lower than the enthalpy of AP solid. This difference in enthalpy can be explained by assuming that the energy difference would be used to pyrolyze the PBAN. However, using the relative weight fractions of the AP and PBAN in the composite propellant, it was calculated that the AP would have to give up 352.3 cal/gm in order to pyrolize the PBAN. Hence it becomes evident that in order to establish the energy content of the two streams it is necessary to know the amount of energy transferred by the three mechanisms stated before and where in the generation of the two streams it is introduced since the chemical kinetics are highly sensitive to temperature variations. In short, to model accurately the propellant burning, not even considering solid phase reactions, it would be necessary to do a complete two-dimensional calculation with kinetics and heat and mass transfer. This task is clearly not within the scope of the present contract.

An alternative to a complete calculation is to assume that the overall combustion process is kinetically controlled since the mixing is very quick and the kinetics are slow at these low pressures. This assumption is standard for low pressure systems such as SPGG; however, the very large grain sizes of the AP crystals cast some doubt on the validity of the quick mixing part of the assumption. If this assumption is accepted, however, then we can assume that the decomposition products of the oxidizer and binder as discussed in Section 2 are injected into an environment of a premixed flame and that the heat transfer necessary to drive the combustion is instantaneous so that the enthalpy of the flame is that of the composite propellant. The composition of the premixed flame is the only unknown quantity left in the process. We shall thus make the further

assumption that the premixed flame can be characterized by an equivalent flame in a well stirred reactor whose length and stay time are the same as those in the overall mixing region in the combustion chamber. The only justification for the last assumption is that it will allow a hopefully reasonable nonequilibrium chemical result with energy being conserved.

In order to perform the calculation as stated the overall mixing length which includes both the primary and secondary diffusion flames must be known. To a first order approximation the overall mixing length is

$$\ell = \tau v_s \tag{3-1}$$

where τ = characteristic time for mixing
v_s = velocity normal to the surface of the propellant

τ is defined for molecular diffusion and convection as:

$$\tau = \frac{d^2}{\mathcal{D}} \quad \text{(diffusion)} \tag{3-2}$$

$$\tau = \frac{d}{V_T} \quad \text{(convection)} \tag{3-2b}$$

where d = distance to mix through
$\mathcal{D}$ = binary diffusion coefficients
V_T = velocity tangent to the propellant surface

Making use of kinetic theory and noting that $d = 1/2\delta$, where δ is equal to the particle diameter, we get:

$$\ell = \frac{\delta^2 (P/P_o) v_s}{\mathcal{D}_o (T/T_o)^{1.76}} \quad \text{(diffusion)} \tag{3-3a}$$

$$\ell = \frac{\delta}{2}\left(\frac{V_s}{V_t}\right) \quad \text{(convection)} \tag{3-3b}$$

The mixing length for pure diffusion is easily calculated to be 24.6 δ for 400 micron particles and 6.15 δ for 200 micron particles. However, in order to calculate the convective mixing length we must estimate the tagential velocity, V_T. Due to the surface roughness and irregular erosion rate the tangential velocity should be on the order of 5 to 10% of the one-dimensional normal velocity. This estimate would yield a mixing length of 5δ to 10δ. It is obvious then that the diffusional mixing length will be the maximum possible for the combustor.

Equation (3-1) is of course only a rough approximation to the real mixing length since it completely ignores variations in concentration and temperature gradients caused by the mixing and combustion. An exact solution of the multi-component diffusion equation is not within the scope of this project, however, we can consider the simpler case of binary diffusion. From Fick's Law the binary diffusion equation without convection is:

$$\rho \frac{\partial x_i}{\partial t} = \nabla \cdot (\rho \mathcal{D} \nabla x_i) \tag{3-4}$$

where ρ = density

x_i = mass fraction of the i^{th} species

$\mathcal{D}$ = binary diffusion coefficient

Noting the similarity between mass diffusion and thermal diffusion, equation (3-4) can be solved numerically using a lumped parameter electrical analog finite difference method as is done in heat transfer problems, see Ref. 21 . This method assumes that the problem can be treated as a finite network of nodes with each node having uniform properties. Under these assumptions equation (3-4) reduces to

$$\frac{dx_i}{dt} = \frac{1}{C_i} \left\{ \sum \frac{x_j - x_i}{R_{ij}} \right\} \tag{3-5}$$

where C_i = capacitance of the i^{th} node

R_{ij} = resistance between node i and j

It can be shown that

$$R_{ij} = \frac{\Delta r_{ij}}{\rho A \beta} \qquad (3\text{-}6)$$

$$C_i = \rho A \Delta r_i$$

where A = cross-sectional area

Δr_{ij} = distance between node i and j

Δr_i = length of node i

If we only consider a simple 2 node system with constant properties, then equation (3-5) reduces to

$$\frac{dx_1}{dt} = \frac{1}{R_{12}C_1}\left((1-x_1)\sigma - x_1\right) \qquad (3\text{-}7)$$

where $\sigma = \frac{\text{volume of node 1}}{\text{volume of node 2}}$

The solution of (3-7) with the boundary conditions

$$x_1(t=0) = 1$$

$$x_2(t=0) = 0$$

is

$$x_1 = \frac{\sigma + e^{-\frac{(1+\sigma)t}{RC}}}{1+\sigma} \qquad (3\text{-}8)$$

The RC product for the 2 node system becomes

$$RC = \frac{\Delta r_{12} \cdot \Delta r_1}{\mathcal{D}}$$

Figure 3-3 shows the results of a computation made using the two node model for a 400μ diameter particle assuming a diffusion coefficient of 1. As can be seen from the figure, there is an appreciable amount of mixing within the first particle diameter and mixing is complete soon after 6 particle diameters.

The two node model predicts a higher initial rate of mixing than will occur in reality due to the high initial concentration gradients. A multi-node model computation was attempted by using a computer program to solve equation (3-5) under the following boundary conditions

$$\left.\frac{\partial x_i}{\partial r}\right|_{r=0} = 0$$

$$\left.\frac{\partial x_i}{\partial r}\right|_{r=r_{fuel}} = 0$$

and assumptions

$$\frac{\partial}{\partial r} >>> \frac{\partial}{\partial z} >> \frac{\partial}{\partial \theta}$$

where r = radial direction
z = normal direction
θ = azimuthal direction

with density being calculated by assuming constant molecular concentration at each node and temperature evaluated from an equilibrium table of O/F versus temperature. The results of the computation were not entirely satisfactory since a very high mixing rate was initially predicted at the

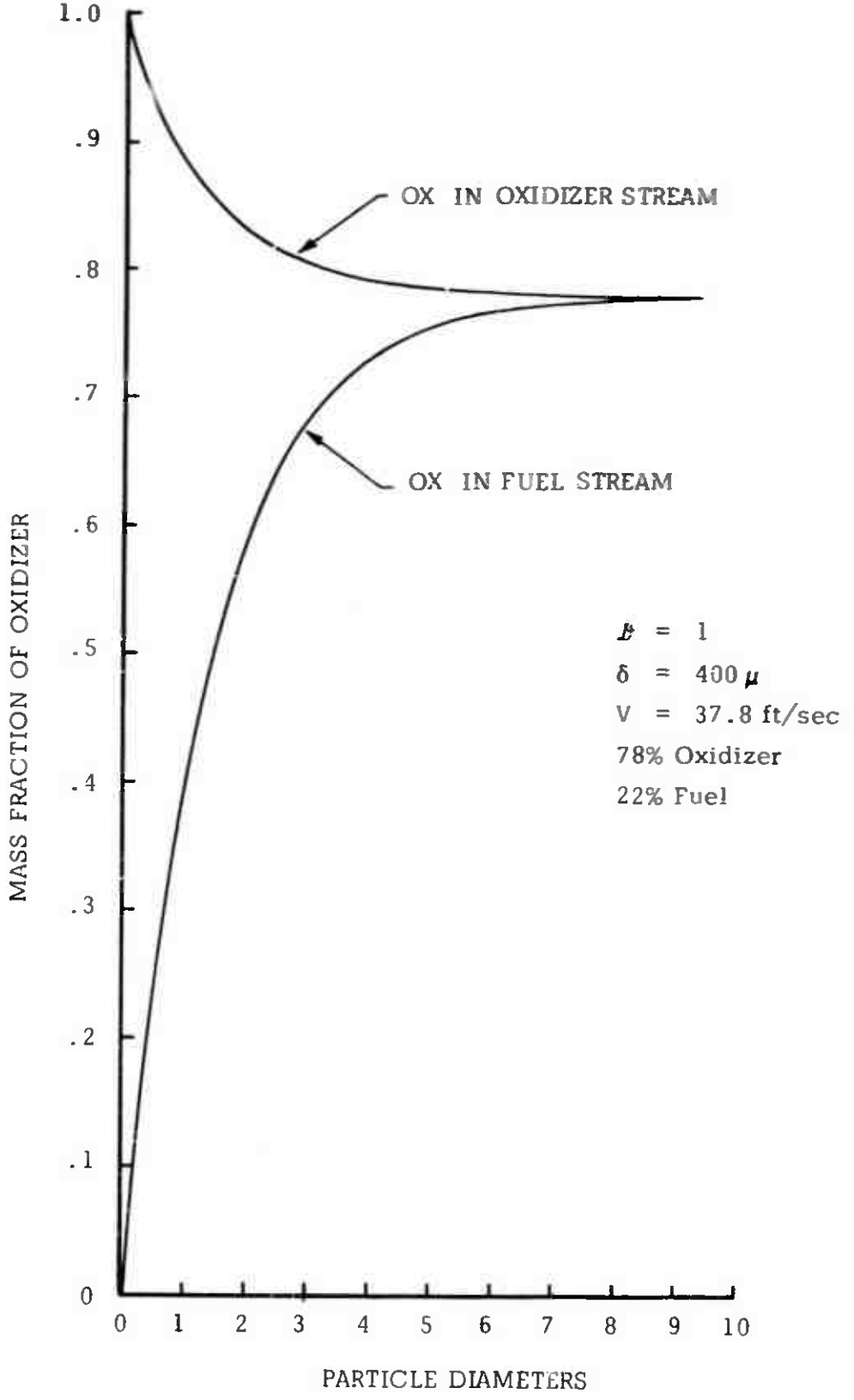

Figure 3-2. RESULTS OF 2 NODE DIFFUSION MIXING MODEL

juncture of the two streams which negates the assumption that the derivatives in the z direction are small. However, the model did predict that the mixing is completed in range of 2000$_\mu$ to 4000$_\mu$ depending on the AP particle size used.

The above results for the mixing length were used to make two stirred reactor runs with reactor lengths of 2400$_\mu$ and 9600$_\mu$ which were the limiting lengths calculated. The results of these stirred reactor calculations were then used as inputs into a streamtube calculation for the chamber and nozzle of the SPGG device. The results of these computations are presented in Section 5 of this report.

Since the stirred reactor model was used to predict the nonequilibrium start conditions in the chamber of the SPGG device, a brief description of the model is presented in Appendix A. Also presented in Appendix A is a description of a shear layer mixing option added to the GKAP computer program under this contract.

In conclusion, the mixing and combustion of the composite propellant used in the SPGG device was studied extensively. The literature was searched and it was found that no satisfactory model of this phenomena existed for the purpose of determining propellant flame structure and composition. Various models were tried, including a pure diffusion model, with little success due to the difficulty and two dimensional nature of the physical problem. In the end a stirred reactor model was adopted since this model allowed for finite rate chemistry while conserving energy between the fuel and oxidizer.

4. SMALL SIGNAL GAIN CALCULATION

The primary purpose of the SPGG device was to determine if laseable species could be produced in quantity in the exhaust plume and the purpose of this contract was to analyze the combustion process in the device and determine the mechanism, if any, which would produce the laseable species.

Experimentally the presence of laseable species is detected by measuring the gain or loss in intensity of a CO_2 laser beam which penetrates the vibrationally excited media. In order to correlate with experimental data and also since the presence of vibrationally excited species does not insure laseability it was necessary to include a small signal gain calculation option into the GKAP computer code.

The definition of the small gain coefficient, α_0, is that if a plane wave of intensity I_0 is propagating in the positive x direction, at $x = x_0$, then the increase or decrease in intensity with x is given by

$$I = I_0 e^{\alpha_0 (x - x_0)} \tag{4-1}$$

the subscript 0 is appended to α to denote this result as the "small signal gain," i.e., the limiting value for $I \to 0$.

The equation for the gain of electromagnetic radiation was originally derived (independently) by Füchtbauer and Fadenberg and was intended to describe absorption. From Refs. 22, 23, and 24 the gain coefficient is given by

$$\alpha_0 = \frac{A_{mn} c^2}{8 \pi \nu^2} g_m \left[\frac{N_{v',m}}{g_m} - \frac{N_{v,n}}{g_n} \right] G(\nu, \nu_{mn}) \tag{4-2}$$

The amplification is associated with transition between two vibrational states, v' and v. The prime denotes the upper energy level. The radiation emitted by the vibrational transfer in energy levels is not monochromatic, but is spread out in frequency from a combination of Doppler broadening, due to

molecular motions, Lorentz broadening, due to collisions, and natural broadening, due to radiation decay. The frequency distribution may be represented by a line shape function, $G(\nu,\nu_{mn})$, which has roughly a bell shape. Of most interest is the line function at the line center since it is a maxima there. For natural and collisional (Lorenz) broadening at the line center,

$$G(\nu,\nu_{mn}) = \frac{2}{\pi(\Delta\nu)_{1/2}} \tag{4-3}$$

where $(\Delta\nu)_{1/2}$ is the full line width at half maximum and is equal to

$$(\Delta\nu)_{1/2} = \frac{\gamma}{2\pi} \quad \text{for natural broadening}$$
(γ = radiation dampening factor)

$$(\Delta\nu)_{1/2} = \frac{Z}{\pi} \quad \text{for Lorenz broadening}$$
(Z = collision frequency)

For Doppler broadening the line function at the line center is

$$G(\nu,\nu_{mn}) = \sqrt{\frac{\ln 2}{\pi}}\ \frac{2}{(\Delta\nu_D)_{1/2}} \tag{4-4}$$

where $(\Delta\nu_D)_{1/2}$ is given by

$$(\Delta\nu_D)_{1/2} = \frac{2\sqrt{2R\ln 2}}{c}\ \nu_0\sqrt{T/M_w}$$

Not included in equation (4-2) or considered here is the variation of the frequency with rotational energy levels, J quantum numbers, and the vibrational-rotational interaction factor. These effects are of second order.

The Einstein A coefficient, A_{mn}, is related to the inverse of the decay time, τ, for the transition from the upper energy level, (v', J_m) to the lower energy

level, (v, J_n). Since the only J dependent part of A_{mn} considered here is the dipole moment of the molecule, then A_{mn} may be written as the product of J dependent and independent parts by introducing the line strength, S_{J_n}, that is,

$$A_{mn} = \frac{S_{J_n}}{g_m} A_v^{v'} \tag{4-5}$$

where $S_{J_n} = J_n$ for P-branch transitions

$= J_n + 1$ for R-branch transitions

$A_v^{v'} = \frac{1}{\tau_v^{v'}}$ = Einstein probability of spontaneous emission corresponding to the integrated band intensity (sec^{-1})

Hence equation (4-2) may be rewritten as

$$\alpha_0 = \frac{A_v^{v'} \lambda^2}{8\pi} S_{J_n} \left[\frac{N_{v',m}}{g_m} - \frac{N_{v,N}}{g_n} \right] G(\nu, \nu_{mn}) \tag{4-6}$$

The degeneracies or statistical weights, g_m and g_n, are given by

$$g_k = (2 J_k + 1) \tag{4-7}$$

since the freedom to rotate about any axis allows $2J+1$ states to have the same energy for a given value of J.

The total number densities of the vibrationally excited species, N_v's, are calculated directly by the GKAP computer program using finite rate chemistry. However, the gain equation requires that the distribution over the rotational energy levels for each vibrational level be known. Since it is well-known that the rotational degrees of freedom in a gas equilibrate rapidly among themselves and with the translational degrees of freedom,

one can reasonably assume that the molecules are distributed over the rotational states according to the Boltzmann distribution with rotational temperature, T_r, equal to the translational temperature, i.e., the "gas temperature." With this assumption the number densities, $N_{v,J}$, within a vibrational state for a given J are

$$N_{v,J} = \frac{N_v}{Q_{rot}} g_J \, \mathrm{EXP}\left(-J(J+1) \frac{B_v hc}{kT}\right) \tag{4-8}$$

where N_v = total number density of the vibrational state (molecules/cc)

B_v = rotational constant (cm^{-1})

h = Planck's constant (erg-sec)

k = Boltzmann's constant (erg/^oK)

c = speed of light (cm/sec)

Q_{rot} = rotational partition function

The rotational partition function for small B and large T has been shown to be

$$Q_{rot} \simeq \left(\frac{kT}{Bhc}\right)/\delta \tag{4-9}$$

where δ = symmetry factor (see Ref. 25 and 26)

For linear symmetric triatomic molecules such as CO_2 the symmetry factor is 2 and reflects the selection rule for such molecules. The selection rule being that for the rotational states only even or odd values of J are allowed for a given vibrational state. The net effect is that the populations for a given J are doubled and hence the small signal gain coefficient is also doubled.

As implemented in the computer program the variation of B with v in equation (4-9) is ignored since the variation is small.

Thus, equations (4-3) or (4-4), (4-6), (4-7), (4-8), and (4-9) are sufficient for the computer program to calculate the gain coefficient given the type of broadening, $A_v^{v'}$, λ, B, and δ for a given J. The program calculates and prints out the maximum value of α_0 for hoth P-branch and R-branch transitions for a given range of J's.

5. RESULTS AND CONCLUSIONS

As stated previously, the purpose of this effort was to analyze the combustion process in the SPGG device to find out the mechanism, if any, which could produce quantities of excited state species sufficient to lase. However, experimental results obtained by the Air Force during the course of the contract showed completely negative results in the measurements of gain. For this reason the emphasis on the work performed under this contract changed from a detailed analysis of the AP/PBAN propellant system of the SPGG device to adding a more general modeling and analysis capability to the GKAP computer code. Thus the analysis of the SPGG device is not totally complete, however, it does show some interesting results and trends.

The mixing and combustion model selected for tne SPGG device, see Section 3, was that of a stirred reactor of a length of the overall mixing zone. The input to the reactor consisted of the decomposition products of the AP and the pyrolysis products of the PBAN as discussed in Section 2. The chemical kinetic reaction scheme of that section was also used as the mechanism within the reactor.

Two stirred reactor runs were made using mixing lengths of 2400μ (6 AP particle diameters) and 9600μ (24 diameters). The results of these calculations and a chemical equilibrium calculation are shown in Table 5-1 for the major thermodynamically stable species.

TABLE 5-1

SPECIE CONCENTRATION
FOR COMBUSTION MODELS

Calculation	SPECIE (MOLE FRACTIONS)					
	CO	CO_2	HCl	H_2	H_2O	N_2
Chemical Equilibrium	.2868	.04006	.138321	.264402	.194377	.073011
Stirred Reactor (2400 μ)	.1897	.0727	.150575	.1567	.2770	.0748
Stirred Reactor (9600 μ)	.20748	.06518	.1497	.1704	.2707	.07507

This table shows a substantial departure from equilibrium for all species for both the 6 and 24 diameter cases. As is expected from a stirred reactor model, the longer the length (stay time), the closer to equilibrium the output composition will be.

Examining the reasons for the non-equilibrium composition, the following becomes clear for the species listed below.

CO_2 and CO

The reaction $CO+ClO \rightarrow CO_2+Cl$ is the dominant mechanism for the overproduction of CO_2 and deficiency of CO. The large excess of ClO being introduced to the reactor causes this reaction to proceed much faster than the other mechanism provided for destroying CO_2 and producing CO.

HCl

The overproduction of HCl is caused by the reaction $Cl+H_2 \rightarrow HCl+H$ which is producing HCl at a rate 3 times faster than the largest HCl oxidation reaction, $HCl+O \rightarrow Cl+OH$, is destroying it. The Cl for this reaction is being produced by $CO+ClO \rightarrow CO_2+Cl$ reaction and the H_2 by the NH_3 reduction reactions, $NH_3+H \rightarrow NH_2+H_2$ and $NH_2+H \rightarrow NH+H_2$. Note that CO, ClO, and NH_3 are input reactants to the reactor.

H_2

The underproduction of H_2 is due mainly to the overproduction of HCl since most of the H_2 produced by the reduction of NH_3 is consumed by the production of HCl.

H_2O

The excess amounts of H_2O are produced by the following reactions with the OH radical which is an input reactant to the reactor

$$CH_2O+OH \rightarrow H_2O+HCO$$
$$H_2+OH \rightarrow H_2O+H$$
$$NH+OH \rightarrow H_2O+N$$

The formaldehyde for the first reaction comes from the oxidation of acetylene

$$C_2H_2+OH \rightarrow CH_2O+CH_3$$

and the H_2 and NH are produced by the reduction of ammonia. Both C_2H_2 and NH_3 are present in large quantities since they are inputs to the reactor.

N_2

The slight excess amounts of N_2 above the equilibrium concentration is due the fact that N_2 is added directly into the reactor and that there are no significant reactions destroying N_2 at these temperatures.

Thus from the above analysis the departure from equilibrium can be attributed to the presence of large quantities of the raw reactants which do not have sufficient time to react at the chamber pressure of the SPGG device. For summary purposes the input reactants and the major reaction mechanisms within the reactor are shown below.

REACTOR KINETIC MECHANISM

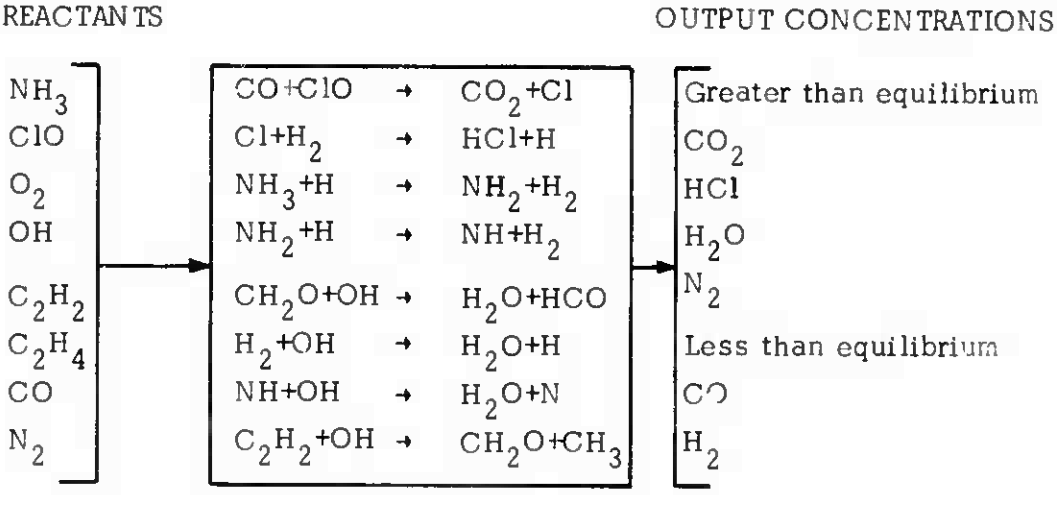

Figure 5-1. STIRRED REACTOR CHEMISTRY

Kinetic stream tube runs were made for the nozzle with a variety of initial conditions ranging from full chemical equilibrium start conditions to the output of the stirred reactor. Departures from chemical equilibrium at the throat plane of the nozzle were noted in all cases and varied from small to large.

In those runs started from equilibrium or close to equilibrium, the flow stayed in or equilibrated rapidly until the vicinity of the throat plane. At approximately an area ratio of 2 the flow experiences a very rapid acceleration from a Mach number of M=.25 to M=1.0 in the distance of 0.5 inches. The high velocities and corresponding short stay times in this region does not allow the chemistry to remain in equilibrium at the low pressures as are characteristic in the SPCG device.

Cases which were run from stirred reactor initial conditions stayed substantially out of equilibrium for the entire time in the nozzle. Table 5-2 lists selected specie concentrations at the throat (also exit) plane of the nozzle for the various cases of interest.

TABLE 5-2

SPECIE CONCENTRATIONS AT THE NOZZLE EXIT PLANE

CASE	SPECIE CONCENTRATIONS (MOLE FRACTIONS)					
	CO	CO_2	HCl	H_2	H_2O	N_2
Full Chem. Eq.	.2824	.04483	.139018	.26976	.190044	.073073
Chem. Eq. Start	.2864	.0404	.1383	.2647	.194096	.073015
Stirred Reactor Start ($L=2400\mu$)	.2308	.05455	.14664	.20136	.2549	.07707

The results of these calculations show that any significant departure from chemical equilibrium will persist throughout the chamber of the device. The most likely reason for this effect is the low chamber pressure of the device since the reaction rates proceed approximately as P^{σ} where σ is the order of the reaction.

However, departure from chemical equilibrium does not necessarily mean that a population inversion has occurred among the vibrationally excited states of a species. For this reason gain calculations were performed on CO_2 for the L=2400μ stirred reactor start case. The excited state CO_2 reaction set is shown in Table 5-3. The results of this calculation showed a small negative gain of about α_0=-.0025 cm^{-1} throughout the entire nozzle for the $CO_2(00^\circ\ 1) \rightarrow CO_2(10^\circ\ 0)$ transition.

In conclusion, the analysis of the SPGG device showed that any substantial departure from chemical equilibrium of the flow in the combustion and mixing zone would not equilibrate by the time the flow had reached the nozzle exit plane. The analysis also showed that there was not a population inversion hetween the (00° 1) and (10°0) vibrational levels of CO_2 despite the large departure from chemical equilibrium. It is felt that the intermediate levels of pressure and temperature (lower than most rocket motors and higher than known laser devices) accounts for this effect. In other words the production rates at these pressures and temperature are not fast enough to produce equilibrium but are too fast to allow an inversion.

TABLE 5-3

EXCITED STATE CO_2 REACTION SET

	RATES*		
	A	N	B (KCALS)
$CO_2(110)+M \rightarrow CO_2(020)+M$**	$.31 \times 10^{-4}$	-4.9	0
$CO_2(110)+M \rightarrow CO_2(100)+M$	.215	-4.2	0
$CO_2(030)+M \rightarrow CO_2(020)+M$	.414	-4.18	0
$CO_2(030)+M \rightarrow CO_2(100)+M$	4.1	-3.6	0
$CO_2(100)+M \rightarrow CO_2(010)+M$	.039	-4.4	0
$CO_2(020)+M \rightarrow CO_2(010)+M$	1.08	-4.0	0
$CO_2(010)+M \rightarrow CO_2(000)+M$	24.4	-3.28	0
$CO_2(001)+M \rightarrow CO_2(110)+M$	2.25	-3.84	0
$CO_2(001)+M \rightarrow CO_2(030)+M$	2.25	-3.84	0
$CO_2(110)+M \rightarrow CO_2(030)+M$	$1.365 \times 10^{+11}$	- .5	0
$CO_2(100)+M \rightarrow CO_2(020)+M$	2.73×10^{12}	- .5	0
$CO_2(001)+CO_2(000) \rightarrow CO_2(100)+CO_2(010)$	6.64	-2.59	0
$CO_2(001)+CO_2(000) \rightarrow CO_2(020)+CO_2(010)$	.0708	-3.05	0
$CO_2(110)+CO_2(000) \rightarrow CO_2(100)+CO_2(010)$	$.43 \times 10^{12}$	- .5	0
$CO_2(030)+CO_2(000) \rightarrow CO_2(100)+CO_2(010)$	$.43 \times 10^{10}$	- .5	0
$CO_2(030)+CO_2(000) \rightarrow CO_2(020)+CO_2(010)$	$.43 \times 10^{12}$	- .5	0
$CO_2(100)+CO_2(000) \rightarrow 2\ CO_2(010)$	$.43 \times 10^{12}$	- .5	0
$CO_2(020)+CO_2(000) \rightarrow 2\ CO_2(010)$	$.43 \times 10^{12}$	- .5	0

* Rates are for left to right and are of the form AT^{-N} EXP(-B/RT)

**All third body reaction rate ratios were taken as 1.0

6. REFERENCES

1. Nickerson, G. R., Frey, H. M., and Coats, D. E., "GKAP - Generalized Kinetics Analysis Program," Dynamic Science Report, June 1971.

2. Johnston, H. S., and Parr, C., "Activation Energies from Bond Energies. I. Hydrogen Transfer Reactions," J. Am. Chem. Soc. 85, 2544 (1963).

3. Evans; M. G., and Polanyi, M., "Inertia and Driving Force of Chemical Reactions," Trans. Faraday Soc. 34, 11 (1938).

4. J. O. Hirschfelder, J. Chem. Phys. 9, 645 (1941).

5. R. Tunder, S. Mayer, B. Cook, and L. Schieler, "Compilation of Reaction Rate Data for Nonequilibrium Performance and Re-entry Calculation Programs," Aerospace Corporation (1966).

6. Jacobs, P. W. M., and Whitehead, H. M., Chem. Revw., 69, 551 (1969).

7. Jacobs and Pearson, Combustion and Flame, 13, 419 (1969).

8. Guigao, C., and Williams, F. A., "A Model for Ammonium Perchlorate Deflagration Between 20 and 100 Atmospheres," AIAA paper No. 71-171, New York, January 1971.

9. Pearson, "The Role of Catalysts in the Ignition and Combustion of Solid Propellants," JANNAF Solid Propellant Combustion Conference, APL, Johns Hopkins, 13-15 October 1970.

10. McHale, E. E., "Combustion Chemistry of AP-based Propellants", Informal note, ECCL file, June 3, 1971.

11. Nagao, M. and Hikata, T., "Fundamental Studies on Combustion of Solid Propellants", Kogyo Kayaku Kyokaihi 27 (4), 234-40 (1966).

12. Sabadell, A. J., J. Wenograd, and M. Summerfield, AIAA J. 3, P1580 (1965).

13. Williams, A., and Smith, D. B., "The Combustion and Oxidation of Acelylene", Chem. Rev., 70, 267 (1970).

14. S. C. Sorenson, et. al., "Ethane Kinetics in Spark-Ignition Engine-Exhaust Gases", Thirteenth Symposium (International) on Combustion, p. 451, The Combustion Institute, 1971.

15. D. T. Baulch, et. al., "High Temperature Reaction Rate Data", The University of Leeds, Vol. No. 1,2,3,4, and 5, May 1968 through July 1970.

16. Nachbar, W., "A Theoretical Study of the Burning of a Solid Propellant Sandwich," ARS Progress in Astronautics and Rocketry, Vol. I: Solid Propellants Rocket Research, Academic Press, New York, 1960, pp 207-266.

17. Beckstead, M. W., Derr, R. L., and Price, C. F., "A Model of Composite Solid Propellant Combustion Based on Multiple Flames," AIAA Journal, Vol. 8, No. 12, December 1970, pp 2200-2207.

18. Summerfield, M. et al., "The Burning Mechanism of Ammonium Perchlorate Propellants," ARS Progress in Astronautics and Rocketry, Vol. I: Solid Propellants Rocket Research, Academic Press, New York, 1960, pp 207-266.

19. Derr, R. L., and Osborn, J. R., "An Experimental Investigation of the Gaseous Phase Reaction Zone in a Composite Solid Propellant," TM-67-6, Jet Propulsion Center, Purdue University, September 1967.

20. Taback, H. J, "The Effects of Several Composition Factors on the Burning Rate of an Ammonium Perchlorate Solid Propellant," Aeronautical Engineering Report No. 429, Princeton University, September 1958.

21. Lockheed, Thermal Analyzer Computer Program for the Solution of General Heat Transfer Problems, Contract No. 9-3349, July 1965.

22. Mitchel, A. C. G. and Zemansky, M. W., Resonance Radiation and Excited Atoms, Cambridge University Press, New York, 1961.

23. Airey, J. R., "Cl+H Br Pulsed Chemical Laser: A Theoretical and Experimental Study", J. of Chemical Physics, Vol. 52, Janaury 1970, pp 156-167.

24. Patel, C. K. N., "Continuous-Wave Laser Action on Vibrational-Rotational Transitions of CO_2", Physical Review, Vol. 136, November 1964, pp A1187-A1193.

25. Penner, S. S., Chemistry Problems in Jet Propulsion, Pergamon New York, 1957.

26. Clarke, J. F., and McChesney, M., The Dynamics of Real Gases, Butterworths, London, 1964.

APPENDIX A - MIXING MODELS

This appendix describes two mixing models used under this contract. Section A-1 describes a stirred reactor model and Section A-2 describes a model for the mixing in a shear layer between two co-flowing streams.

A-1 Stirred Reactor Model

In a stirred reactor model reactants enter a reactor and are assumed to be instantly and completely mixed with the products in the reactor. The combustion products extracted from the reactor are thus the same as those in the reactor and only depend on the input reactants and the average stay time in the reactor. This model is particularly useful since it represents the limiting case where fluid physics processes are so fast as to make the chemistry clearly the rate controlling step.

In the steady state process the amount of mass in the reactor does not change and hence continuity becomes

$$\dot{m}_{in} = \dot{m}_{out} \qquad \text{(A-1.1)}$$

The mass flow into the reactor is known and consists of species whose mass fractions are

$$c_{k\,in} = (\rho_k / \rho)_{in}$$

The input enthalpy/unit mass, h_{in}, is known, i.e.

$$h_{in} = \sum (c_k h_k)_{in} + \frac{v_{in}^2}{2} \qquad \text{(A-1.2)}$$

and the stirred reactor will be operating at a known pressure, P. The flow into the reactor will be the sum of the flow rate for each species component

$$\dot{m}_{in} = \sum (c_k \dot{m})_{in} \qquad \text{(A-1.3)}$$

The flow is instantly stirred and then reacted within the reactor which has a fixed volume, V. There is then a mean residence time, τ, within the reactor which depends on the flow rate through the reactor and the amount of mass in the reactor. The change in species concentration due to chemical reactions which occur within a time, τ, is known to be (see Section 2.0, equation (1) of Ref. A-1.)

$$\Delta c_k = \left(\frac{\dot{\omega}_k}{\rho}\right) \tau \qquad \text{(A-1.4)}$$

where

$$\dot{\omega}_k = m_{w_k} \sum_{j=1} \rho^{\sum_{i=1} \nu_{ij}} (\nu'_{kj} - \nu_{kj}) X_j$$

= is the net species production rate for each component species.

Since the mixture is instantly stirred, $\dot{\omega}_k$, will be constant throughout the reactor. See reference A-1 for a more complete discussion of the chemical rate equations. Specie continuity thus requires that for each species

$$\dot{m} c_{k\,out} = \dot{m} c_{k\,in} + \dot{m} \Delta c_k \qquad \text{(A-1.5)}$$

and a stirred reactor calculation consists of finding species concentrations at the outlet of the reactor such that the above system of non-linear simultaneous equations are satisfied. For a system containing N species equations (A-1.2) and (A-1.5) define N+1 non-linear equations with N+1 unknowns (c_k, T). Solutions to the above equations are thus not necessarily unique. However, for a sufficiently small residence time ($\tau \to 0$) a chemically frozen mixture ($\Delta c_k = 0$) will give a solution. For very large residence time ($\tau \to \infty$) a chemical equilibrium mixture ($\omega_k = 0$) will give a solution.

In the CHAP computer program the set of non-linear equations is solved by integrating the differential equations below until the derivatives become zero.

$$\frac{dc_j}{dx} = \dot{S}_j - \dot{m} c_j + \frac{\dot{m}_a}{\dot{m}} \qquad \text{(A-1.6)}$$

$$c_p \frac{dT}{dx} = \dot{H} - \dot{m} h_T - \frac{N}{\sum_{j=1}} h_j \frac{dc_j}{dx} \qquad \text{(A-1.7)}$$

where using the nomenclature above

$$\dot{S}_j = \dot{m} c_{j\,in}$$

$$\frac{\dot{m}_a}{\dot{m}} = \sum c_k$$

$$\dot{m} c_j = \dot{m} c_{j\,out}$$

$$\dot{H} = \dot{m} \left(\sum c_j h_j + \frac{v^2}{2} \right)_{in}$$

$$h_T = \sum c_j h_j + \frac{v^2}{2}$$

It can be seen that when equations (A-1.6) and (A-1.7) are integrated until they reach steady-state, i.e., $\frac{d}{dx} = 0$, that they reduce to equations (A-1.2) and (A-1.5).

A-2 Co-flowing Stream Tube Mixing Model

An option was incorporated into the CHAP computer code to model approximately the mixing between two co-flowing reacting gas streams. The model assumes that all of the mixing between the components of the two streams occurs in the shear layer which develops between the two streams as shown below.

SHEAR LAYER MIXING MODEL

In actuality the phenomena of mixing in the shear layer is highly two dimensional and any simple one dimensional model should be used with care, e.g., see Ref. A-2.

References A-3 and A-4 have shown that the growth of the shear layer between 2 planar jets, co-axial jets, and co-flowing streams is governed by the growth law

$$b = kx^N \qquad \text{(A-2.1)}$$

where

b	=	width of the shear layer
k	=	constant
x	=	distance
N	=	1/2 for laminar flow
	=	1 for turbulent flow

In order to approximate shear layer mixing we consider 3 stream tubes, the two primary streams and one stream tube which contains a small fraction of the total flow which is considered initially mixed. Then Equation (A-2.1) can be rewritten as

$$b = b_0 + k(x - x_0)^N \qquad \text{(A-2.2)}$$

where

b_0 = width of the initially mixed stream tube, i.e., the width of the shear layer at x_0.

If it is assumed that mass is entrained into the shear layer directly proportional to the ratio of the area of the shear layer to the area of the primary streams, then the problem of mass, energy, momentum, and species addition to the shear layer reduces to the simple geometric relationships given below:

planar flow

$$\dot{m} = \frac{\alpha(1-\beta)}{\beta} \frac{kN(x-x_0)^{N-1}}{(r_i - b_{i0})} \qquad \text{(A-2.3)}$$

where r_i = height of the ith primary stream

b_{i0} = height of the shear layer protruding into the ith primary stream at x_0

α = fraction of the total mass flux in the ith primary stream

β = fraction of the total mass flux assigned initially to the shear layer

co-axial case (inner stream tube)

$$\dot{m} = \frac{\alpha(1-\beta)}{\beta} \frac{2(r_1 - b_1)\ kN(x - x_0)^{N-1}}{(r_1 - b_{10})^2} \qquad \text{(A-2.4)}$$

where r_1 = radius of the inner stream tube

b_1 = height of the shear layer proturding into the inner stream

co-axial case (outer stream tube)

$$\dot{m} = \frac{\alpha(1-\beta)}{\beta} \frac{2(r_1 + b_2)\ kN\ (x - x_0)^{N-1}}{r_2^2 - (r_1 + b_{20})^2} \qquad \text{(A-2.5)}$$

where r_2 = radius of the outer stream tube

b_2 = height of the shear layer protruding into the outer stream

for all cases

$$\dot{M} = \dot{m}v \qquad \text{(A-2.6)}$$

$$\dot{H} = \frac{\dot{m}}{Jg}\left(h + \frac{v^2}{2}\right) \qquad \text{(A-2.7)}$$

$$\dot{S}_i = \dot{m}c_i \qquad \text{(A-2.8)}$$

In the above equations $\dot{m}$, $\dot{M}$, $\dot{H}$, and $\dot{S}_i$ are the contribution to the mass, momentum, energy, and species addition rates respectively of the shear layer from one of the primary streams. For usage of this option in the computer program, the reader should refer to Ref. A-1.

REFERENCES

A-1. Nickerson, G. R., Frey, H. M., and Coats, D. E., "GKAP-Generalized Kinetics Analysis Program," Dynamic Science Report, June 1971.

A-2. Lock, R. C., "The Velocity Distribution in the Laminar Boundary Layer Between Parallel Streams." Quarterly J. Mech. and Appl. Math. 4, 42 (1951).

A-3. Schlichting, H., Boundary Layer Theory, McGraw-Hill, 1960.

A-4. Abramovich, G. N., The Theory of Turbulent Jets, MIT Press, 1963.

APPENDIX B

SUMMARY OF RESULTS FOR H/F and D/F IGNITION COMPUTATIONS

In order to demonstrate the use of the GKAP computer code as applied to a problem of current interest to AFRPL a study of the $H_2/F_2/He$ ignition was performed. The study included

Run #1 : A basic $H_2/F_2/He$ (ground state reaction mechanism) ignition calculation

Run #2 : The effect of Deuterum substitution on the ignition

Run #3 : The effect of considering excited state HF (vibrational level ≤ 5) during the ignition calculation.

Results of these computations are summarized below:*

Run #1 : Adiabatic ignition of $H_2/F_2/He$ at constant pressure. The initial concentrations and conditions as well as the reaction mechanism are presented in Table 1. The calculation was continued to "Equilibrium" (at equilibrium derivatives of T & C_i with respect to time will be zero).

Table 2 presents a comparison of an ideal Pressure-Enthalpy Equilibrium calculation with the results of the kinetic calculation after ~ 7.91 millisec. As can be observed from Table 2, the kinetics calculation predicts the equilibrium conditions to within 0.1%.

Figure 1 presents the temperature profiles vs. time for all three calculations. As can be observed from Figure 1, the ground state $H_2/F_2/He$ ignition model for initial T=300°K predicts a 4.625 millisec ignition delay.

An interesting aspect of all three calculations may also be observed in Figure 1. Although the final "equilibrium" Temperature is ≈ 1760°K, during 17 μ sec. the temperature exceeds 2000° K and has a maximum of ≈ 3000°K. This temperature overshoot is due to a lag in the dissociation of the excess F2. Figure 2 presents the reaction net production rates during the actual ignition. As can be observed from Figure 2, the F2 dissociation

*Approximately one minute of CDC 6600 computer time is required for each run.

lags the actual ignition and requires 5-10 μ sec. to absorb the excess energy via dissociation. A sample calculation showing the mechanism and the results of simple hand calculations further illustrates the actual temperature overshoot mechanism and is

Run #2 : Adiabatic ignition, at constant pressure for the same conditions as Run #1 with Deuterium exchanged for the Hydrogen (see Table 3).

Figure 1 presents the temperature profile vs. time for this calculation. The observed ignition delay is 32.798 millisec. The computer run max paged after 32.81 millisec and was not restarted. This ignition delay may be compared with 4.625 millisec for the corresponding H2 condition, i.e. ignition delay ratio:

$$\frac{\tau_{D2}}{\tau_{H2}} = \frac{32.798}{4.625} = 7.1$$

It is interesting to note that the reaction mechanism for the F2 dissociation remains unchanged from Run #1 but the "ignition" reactions have been slowed via D substitution for H. Therefore the relative rate at which F2 may dissociate and absorb excess energy due to ignition, should increase. This should then reduce the temperature overshoot. In fact a reduction of 227°K in peak temperature below the Run #1 peak temperature is calculated.

Run #3 : Adiabatic, constant pressure ignition for $H_2/F_2/He$ including vibrationally excited HF ($v \leq 5$). The initial mole fractions and and reaction mechanism are presented in Table 4.

Figure 1 presents the temperature profile vs. time for this calculation. The observed ignition delay is 6.0 millisec as compared with a 4.625 millisec delay for the ground state mechanism.

The observed difference in ignition delay may be caused by the HF exothermic production producing vibrationally excited HF with resultant lesser energy channeled into thermal energy. This would lengthen ignition delay. However, differences in the reaction rate constants make this unclear.* For example:

a) $2H \rightleftarrows H_2$ Run #1 $k = 1.0\ 10^{18}\ T^{-1}$

$2H \rightleftarrows H_2$ Run #3 $k = 2.5\ 10^{18}\ T^{-1}$

b) $H + F2 \rightleftarrows HF + F$ Run #1 $k = 1.21 \cdot 10^{14}\ e^{-(\frac{2.400}{RT})}$

$H + F_2 \rightleftarrows HF + F$ Run #3 $= \sum$ all reax for HF(0-5)

Run #3 $\sum = .8\ 10^{14}\ e^{(-\frac{2.400}{RT})}$

No attempt was made to determine effects of changes in reaction rates on ignition delay.

Figure 3, presents the HF(0-5) mole fractions vs. time for Run #3. As can be observed from Figure 3, an overproduction of all vibrational levels does occur, in the same manner as observed for the ground state reaction mechanism for Run #1.

One should note that the maximum temperature observed in Run #3 = 3006° K compared to 2997°K for Run #1. This demonstrates that the temperature overshoot is nearly independent of the vibrational reaction mechanism.

*Reaction rates for Run #3 were taken from Kerber & Whitier whereas for Run #1 and #2 rates used were supplied by AFRPL for the purpose of duplicating results obtained with the Aerospace NEST Computer Program.

Reference: Kerber, R.L. and Whittier J. S., "The Effects of Various Parameters on the Behavior of the Pulsed HF Chemical Faser, Aerospace Report No. TOR-0059 (6753-10)-1, 70 December 15.

In addition to the three computer runs discussed above, a series of computer runs were also made for the purpose of examining the effect on $H_2/F_2/H_e$ ignition delay, τ, with varying initial temperature, T_0. Results of these runs, which repeat Run #1 with

$$T_0 = 300, 400, 500, 1000°K$$

are shown in Figure 4, which gives Temperature vs. time for the above initial temperature values. Shown in Figure 5 is a plot of ignition delay, τ, vs. $1000/T_0°K$ which can be seen to be nearly linear.

Simplified Explanation of H_2/F_2 Ignition Results

In order to check the results of the computer calculations of Run #1 it can be assumed that the H_2/F_2 ignition proceeds in essentially two steps:

Step 1)

$$H_2 + F \rightleftarrows HF + H$$

$$F_2 + H \rightleftarrows HF + F$$

Step 2)

$$F_2 \rightleftarrows 2F$$

The Step 1 reactions proceed much faster than Step 2 which is the dissociation of F by third body collisions. Assuming the above two step process, the temperature overshoot can be explained by the following calculation:

For Step 1 the result can be written as

$$M(H_2) + M(F_2) + N(F_2) \rightleftarrows 2M(HF) + N(F_2)$$

For Step 2 the equilibrium result can be written as

$$N(F_2) \rightleftarrows (N-\delta)\ (F_2) + 2\,\delta(F)$$

Discussion of Step 1

Initial conditions were specified in mole fractions of H_2 and F_2 such that

$$M = .159 \qquad M = .159 \text{ mole } H_2$$
$$N = .302 \qquad M + N = .461 \text{ mole } F_2$$

Thus Step 1 gives a mole fraction of HF of

$$HF = .318$$

i.e.

$$.159\ H_2 + .159\ F_2 + .302\ F_2 = .318\ HF + .302\ F_2$$

The average values for C_p and M_w of the mixture over Step 1 are

$$\overline{C}_p = .36 \text{ cal/g-}^\circ \text{K}$$
$$M_w = 19 \text{ g/mole}$$

so that since 1 mole of HF has a heat of formation of

$$\Delta H_f^\circ = -64800 \text{ cal/mole}$$

then the temperature rise of the mixture after Step 1 (producing .318 moles of HF) would be approximately

$$\Delta T = \frac{\Delta H}{\overline{C}_p}$$

where

$$\Delta H = .318 * 64800 \text{ cal/mole}$$
$$\overline{C}_p = .36 * 19 \text{ cal/mole } ^\circ \text{K}$$

so that

$$\Delta T = \frac{20600 \text{ cal/mole}}{6.84 \text{ cal/mole } ^\circ \text{K}}$$

$$\Delta T = 3010^\circ \text{ K}$$

Run #1 gives a temperature rise of 2700° K after 4.625 millisec. During this time the species production rates of Step 1 are approximately 10^2 to 10^3 faster than the rate for Step 2.

Discussion of Step 2

The kinetic calculations of Run #1 proceed to chemical equilibrium and give

$$\delta = .228$$

so that Step 2 gives

$$.302\ (F_2) = .074(F_2) + .456(F)$$

The average values for C_p and M_w of the mixture over Step 2 are

$$\overline{C}_p = .385$$

$$M_w = 16.8$$

so that since 1 mole of F has a heat of formation of

$$\Delta H_f^\circ = 16500 \text{ cal/mole}$$

then the temperature change of the mixture after Step 2 (producing .456 moles of F) would be approximately

$$\Delta T = \frac{\Delta H}{\overline{C}_p}$$

where

$$\Delta H = -.456 * 16500 \text{ cal/mole}$$

$$\overline{C}_p = .385 * 16.8 \text{ cal/mole}^\circ K$$

so that

$$\Delta T = \frac{-7520 \text{ cal/mole}}{6.47 \text{ cal/mole}^\circ K}$$

$$\Delta T = -1160^\circ K$$

Run #1 gives a temperature drop during Step 2 of 1240° K.

The above simplified analysis shows that the kinetic calculations of Run #1 give results which are qualitatively correct, including the observed temperature overshoot during ignition.

TABLE 1

H2/F2/HE Ignition Calculation Constant Pressure

Initial Conditions

$P = 0.42877$ ATM

$T = 300°$ K

Species Mole Fractions

H	0.0
HE	0.38
F	2.0E-7
HF	0.0
H2	0.159
F2	0.461

Reactions (Rate Constant supplied by AFRPL)*

1.	H + H	→	H2	k_1	$= 1.0 \cdot 10^{18} T^{-1}$
2.	F2	→	F + F	k_2	$= 5.0 \cdot 10^{13} e^{-(\frac{35.300}{RT})}$
3.	HF	→	H + F	k_3	$= 4.7 \cdot 10^{18} T^{-1} e^{-(\frac{134.100}{RT})}$
4.	F2 + H	→	HF + F	k_4	$= 1.21 \cdot 10^{14} e^{-(\frac{2.400}{RT})}$
5.	H2 + F	→	HF + H	k_5	$= 1.60 \cdot 10^{14} e^{-(\frac{1.600}{RT})}$

Reactions 1, 2, 3 contain a generalized third body.

*units (cc, mole, sec, °K, kcal)

TABLE 2

RUN #1

Comparison of Equilibrium Calculation and Kinetic Calculation at Time = 7.91 millisec.*

		Mole Fractions					
	T° K	H	HE	F	HF	H2	F2
Equilibrium	1607	0	.2932	.4570	.2453	0	.0045
Kinetic	1603	10^{-13}	.2933	.4562	.2455	10^{-18}	.0050
Difference	4	0	-.0001	+.0008	-.0002	0	-.0005

*The equilibrium results were computed using the NASA/Lewis Research Center chemical equilibrium computer program. The results for Run #1 shown here differ from Figure 1 in that the heat of formation of F was taken as 16.5 rather than 18.8K cal/mole so as to be consistent with the value used in the NASA/LRC program.

The equilibrium temperature for the kinetic calculation has been corrected from 1598° K to 1603° K by reducing the velocity from 19.1 ft/sec to zero as follows:

$$19.1 \frac{\text{ft}}{\text{sec}} \quad => \frac{1.6 \frac{\text{cal}}{\text{g}}}{.33 \frac{\text{cal}}{\text{g} - {}^\circ\text{K}}} \approx 4.9^\circ \text{K}.$$

Kin Temp. corrected to 0 velocity = 1598.0 + 4.9 = 1602.9

TABLE 3

RUN #2

D2/F2/HE Ignition Calculation Constant Pressure

Initial Conditions

P = 0.42877 ATM

T = 300° K

Species Mole Fractions

D	0.0
HE	0.38
F	2.0E-7
DF	0.0
D2	0.159
F2	0.461

Reactions (Rate Constant supplied by AFRPL)*

1.	D + D	→ D2	$k_1 = 0.3 \cdot 10^{18} T^{-1}$
2.	Same as Run #1		
3.	DF	→ D + F	$k_3 = 0.47\ 10^{19}\ T^{-1}\ e^{-(\frac{136.800}{RT})}$
4.	F2 + D	→ DF + F	$k_4 = 0.2\ 10^{14}\ e^{-(\frac{2.400}{RT})}$
5.	D2 + F	→ DF + H	$k_5 = 0.16\ 10^{14}\ e^{-(\frac{1.600}{RT})}$

reactions 1, 2, 3 contain a generalized third body

*units (cc, mole, sec, °K, kcal)

TABLE 4

Rates are right to left from Kerber & Whitmer

```
REACTIONS          H2/F2 EXCITED VIB UP TO 5
 H2 = 2*H          . A=2.5E18.    N=1.0.   B=0.0.    1,2,3
 2*F = F2          . A=3.0E12.    N=0.0.   B=27.3.   4
 H+F = HF(0)       . A=5.0E22.    N=2.0.   B=134.0.  5
 H+F = HF(1)       . A=5.0E22.    N=2.0.   B=122.87. 6
 HF(0) = HF(1)     . A=1.5IE7.    N=-1.455.B=0.0.    14,15
 HF(0) = HF(1)     . A=1.1*E-2.   N=-3.65.  B=0.0.   15
 HF(1) = HF(2)     . A=2.52E7.    N=-1.455. B=0.0.   17,18
 HF(1) = HF(2)     . A=2.3*E-2.   N=-3.65.  B=0.0.   19
 HF(2) = HF(3)     . A=4.5*E7.    N=-1.455.B=0.0.    20,21
 HF(2) = HF(3)     . A=3.57E-2.   N=-3.65.  B=0.0.   22
 HF(3) = HF(4)     . A=6.1*E7.    N=-1.455.B=0.0.    23,24
 HF(3) = HF(4)     . A=4.7*E-2.   N=-3.65.  B=0.0.   25
 HF(4) = HF(5)     . A=7.5*E7.    N=-1.455.B=0.0.    26,27
 HF(4) = HF(5)     . A=5.9*E-2.   N=-3.65.  B=0.0.   28
 H+F   = HF(2)     . A=5.0E22.    N=2.0.   B= 111.34,37
 H+F   = HF(3)     . A=5.0E22.    N=2.4.   B= 101.43,38
END THR REAX
 HF(0) + H = F + H2.  A=7.0E12.   N=0.0.   B=1.71.    7
 HF(1) + H = F + H2.  A=14.0E12.  N=0.0.   B=1.71.    8
 HF(2) + H = F + H2.  A=7.0E13.   N=0.0.   B=1.71.    9
 F + H2 = HF(3) +H .  A=3.0E12.   N=-.5.   B=0.0.     10
 F + H2 = HF(4) +H .  A=3.0E12.   N=-.5.   B=0.0.     11
 F + H2 = HF(5) +H .  A=3.0E12.   N=-.5.   B=0.0.     12
 HF(0)+HF(2)=2*HF(1).A=2.0E4.     N=-2.2.  B=0.0.     38
 HF(1)+HF(3)=2*HF(2).A=2.0E4.     N=-2.2.  B=0.0.     39
 HF(2)+HF(4)=2*HF(3).A=2.0E4.     N=-2.40. B=0.0.     40
 HF(3)+HF(5)=2*HF(4).A=2.0E4.     N=-2.40. B=0.0.     41
 HF(0)+HF(3)=HF(1)+HF(2).  A=6.25E1.  N=-2.8.  B=0.0.    45
 HF(1)+HF(4)=HF(2)+HF(3).  A=6.25E1.  N=-2.8.  B=0.0.    46
 HF(2)+HF(5)=HF(3)+HF(4).  A=6.25E1.  N=-2.8.  B=0.0.    47
 HF(0)+HF(4)=HF(1)+HF(3).  A=3.0E-3.  N=-3.9.  B=0.0.    51
 HF(1)+HF(5)=HF(2)+HF(4).  A=3.0E-3.  N=-3.9.  B=0.0.    52
 HF(0) + F = H + F2.       A=5.0E12.  N=0.0.   B=2.40.   60
 HF(1) + F = H + F2.       A=5.0E12.  N=0.0.   B=2.40.   61
 HF(2) + F = H + F2.       A=10.0E12. N=0.0.   B=2.40.   62
 HF(3) + F = H + F2.       A=10.0E12. N=0.0.   B=2.40.   63
 HF(4) + F = H + F2.       A=20.0E12. N=0.0.   B=2.40.   64
 HF(5) + F = H + F2.       A=30.0E12. N=0.0.   B=2.40.   65
LAST REAX
```

```
THIRD BODY RATE RATIOS
SPECIES H2, 4*1.0,1.0,1.0,1.0,1.0,1.0,1.0,1.1.1.
SPECIES H, 8,3*1,  0,1,0,1,0,1,0,1,0,1,0,1,1,1,
SPECIES F, .4,3*1, 0,1,0,1,0,1,0,1,0,1,1,1,
SPECIES F2 ,  .4,1,1,1,1,0,1,0,1,0,1,0,1,0,1,1,
SPECIES HF(0),.4,1,1,1,1,0,1,0,1,0,1,0,1,0,1,1,
SPECIES HF(1),.4,1,1,1,1,0,1,0,1,0,1,0,1,0,1,1,
SPECIES HF(2),.4,1,1,1,1,0,1,0,1,0,1,0,1,0,1,1,
SPECIES HF(3),.4,1,1,1,1,0,1,0,1,0,1,0,1,0,1,1,
SPECIES HF(4),.4,1,1,1,1,0,1,0,1,0,1,0,1,0,1,1,
SPECIES HF(5),.4,1,1,1,1,0,1,0,1,0,1,0,1,0,1,1,
SPECIES HE,.4,3*1, 0,1,0,1,0,1,0,1,0,1,1,1,
LAST CARD
```

SPECIES MOLE FRACTIONS	
H2	.159
H	0.0
F	0.0000-02
F2	.461
HF(0)	0.0
HF(1)	0.0
HF(2)	0.0
HF(3)	0.0
HF(4)	0.0
HF(5)	0.0
HE	.380

$H_2/F_2/HE$	See Reaction Table 1
$D_2/F_2/HE$	See Reaction Table 2
$H_2/F_2/HE$	(HF v ≤ 5) See Reaction Table 3

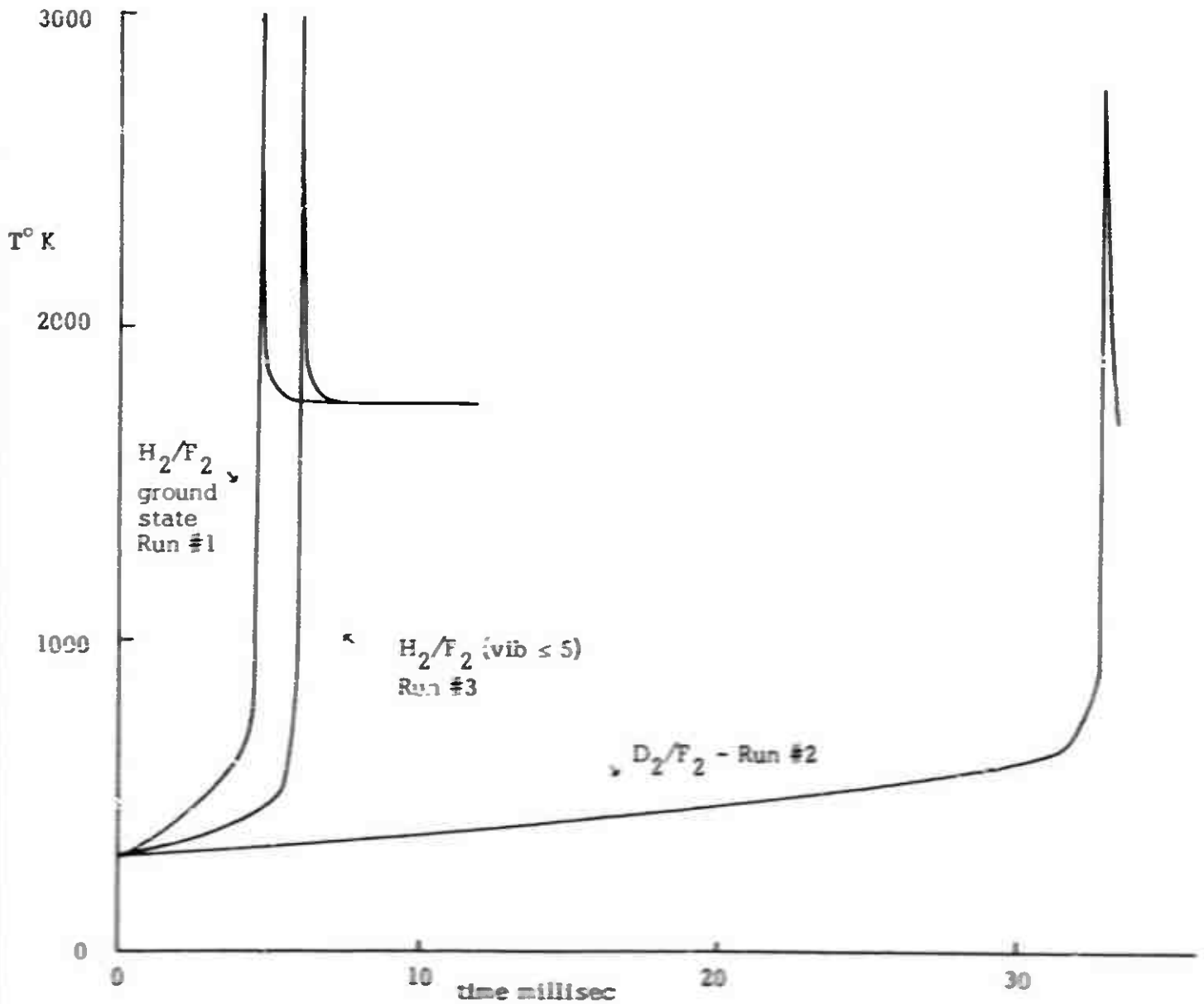

Figure 1. Temperature vs. Time for Runs #1, #2, #3.

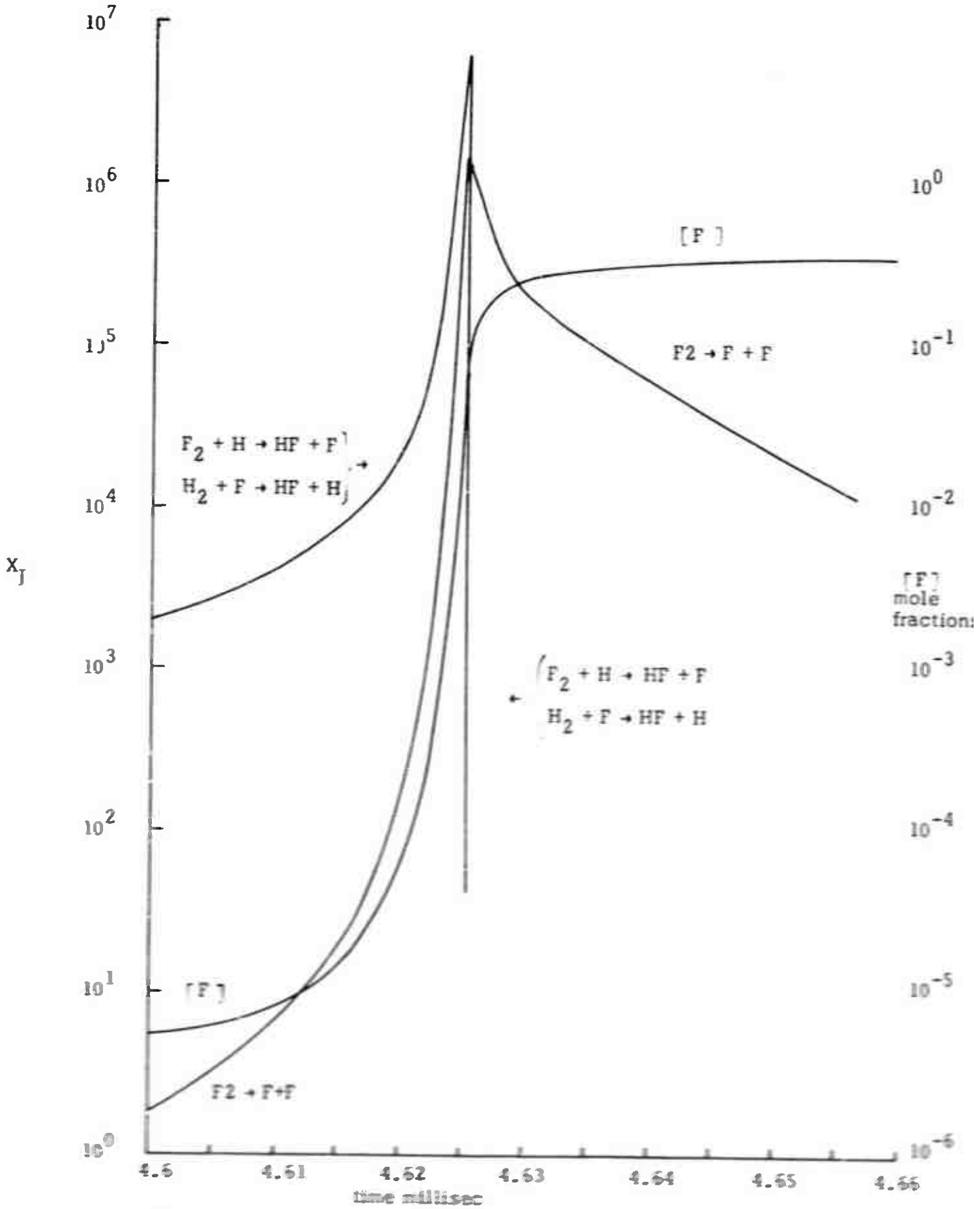

Figure 2. Reaction Net Production Rates, X_J, vs. Time During $H_2/F_2/HE$ Ignition (Run #1). Also Shown is F Species Concentration vs. Time.

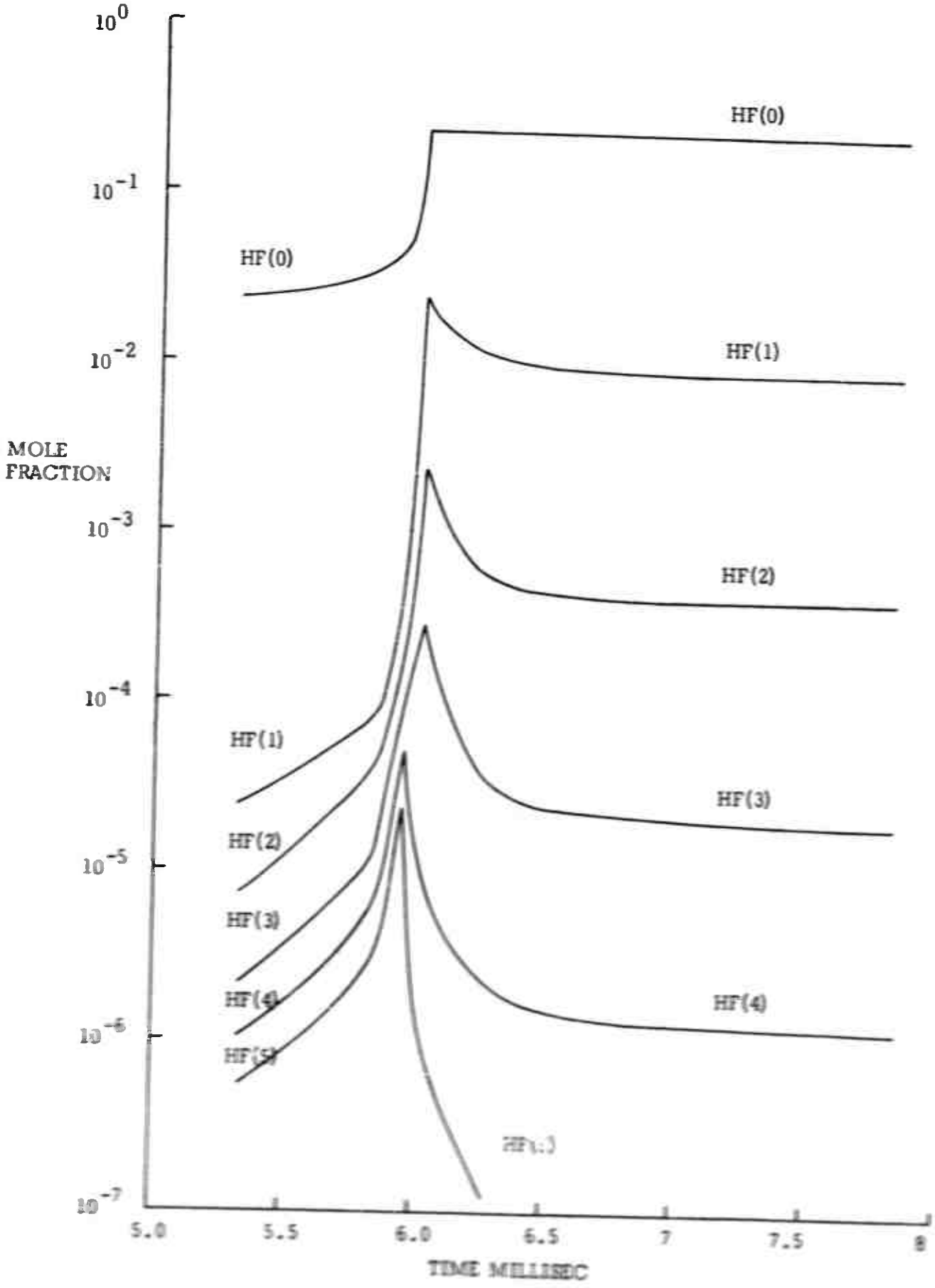

Figure 3. Mole Fractions vs. Time for Excited State HF During Ignition (Run #3)

T_0 °K	$\frac{1000}{T}$	τ
300	3.33	0
400	2.5	1.71
500	2.	2.88
1000	1.	4.62

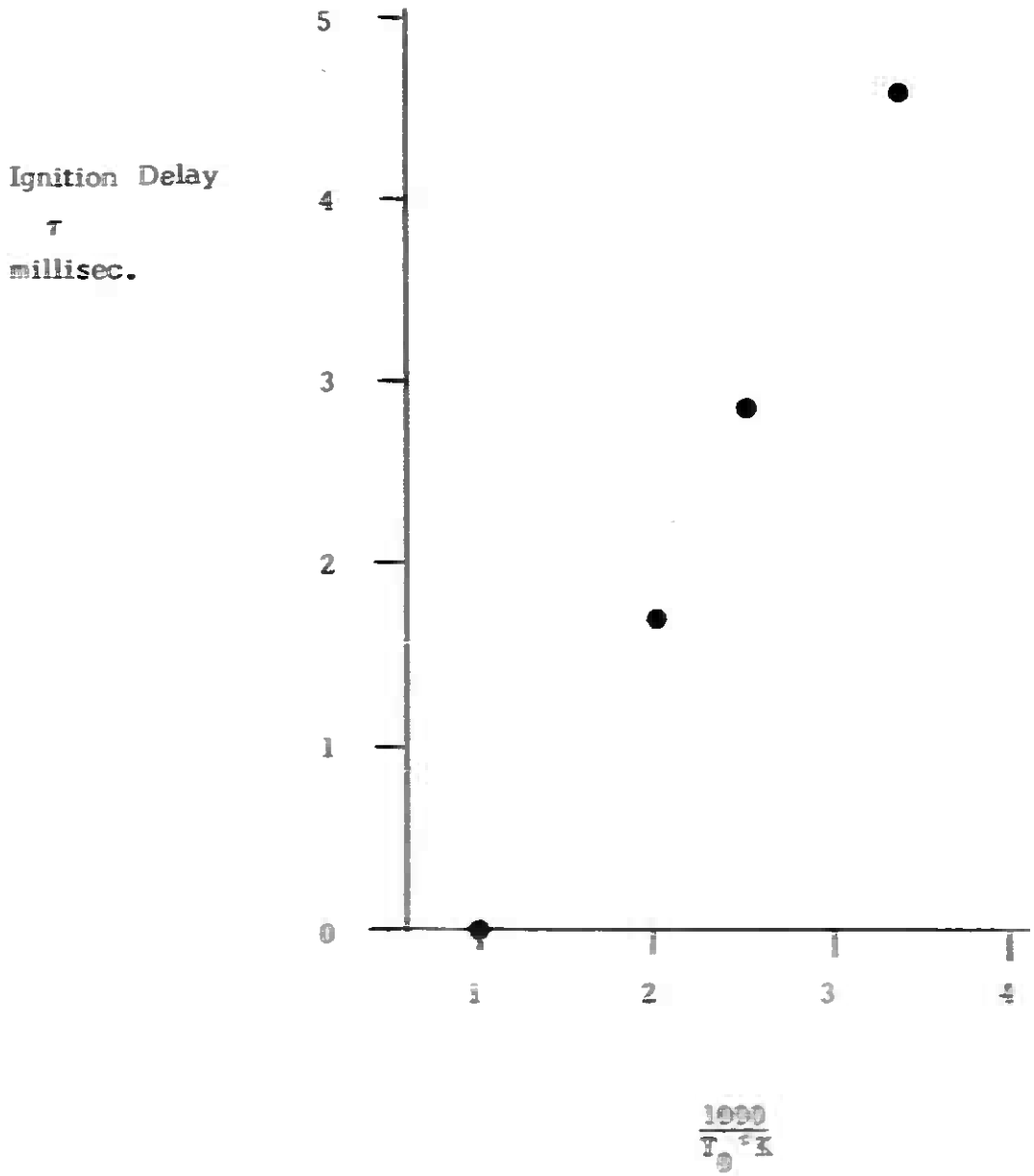

Figure 4: The Effect of Initial Temperature on Ignition Delay for $H_2/F_2/He$ - $[F]_0 = 2 \cdot 10^{-7}$

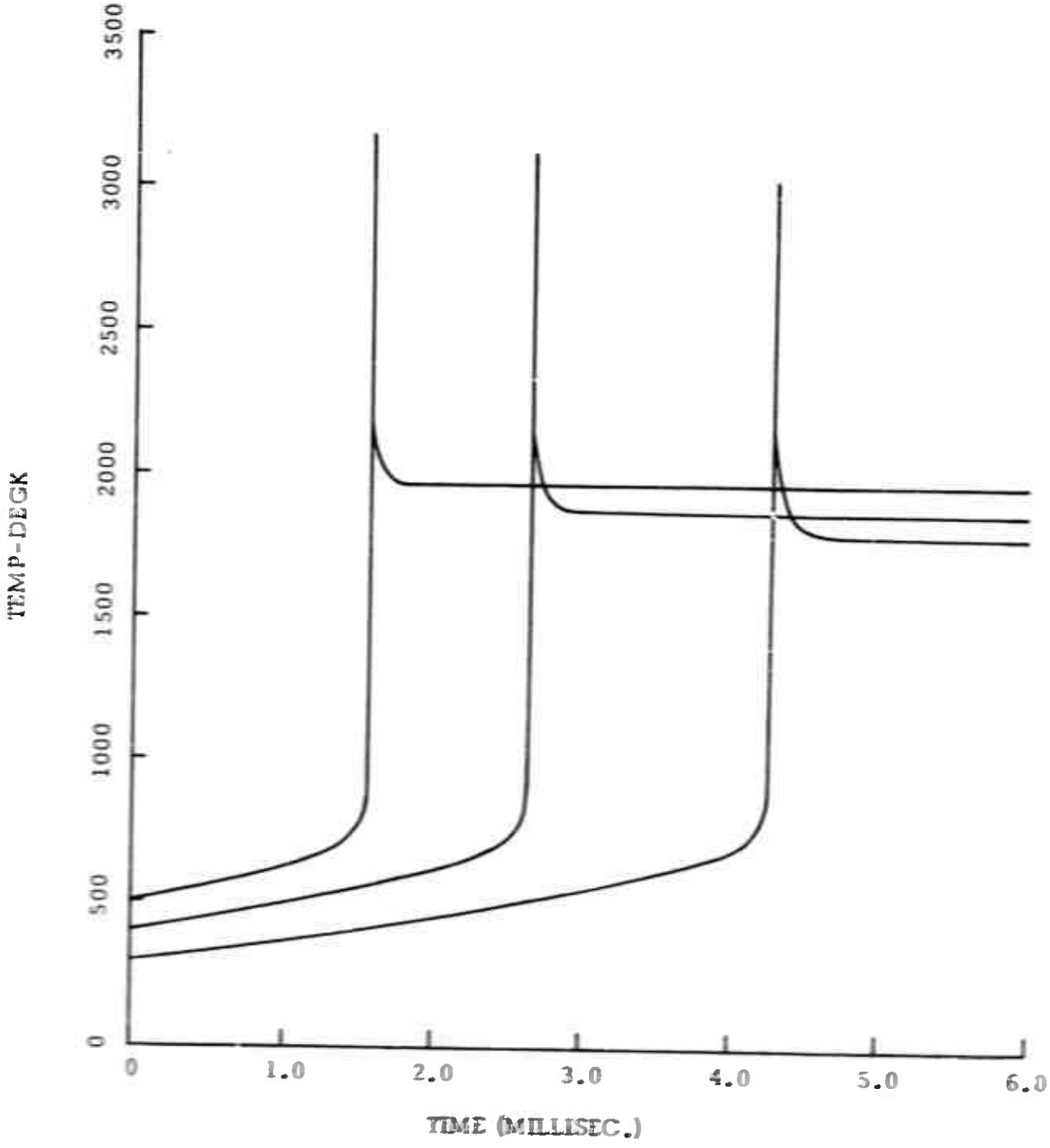

Figure 5: H2/F2/HE Ignition T_0 = 300, 400, 500°K